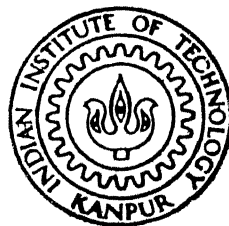


AXIAL FATIGUE BEHAVIOUR OF KEVLAR FABRIC REINFORCED EPOXY RESIN COMPOSITES

by

SANJAY KUMAR MAZUMDAR



DEPARTMENT OF MECHANICAL ENGINEERING

INDIAN INSTITUTE OF TECHNOLOGY, KANPUR

AUGUST 1988

ME

1988

M

MAZ

AXI

AXIAL FATIGUE BEHAVIOUR OF KEVLAR FABRIC REINFORCED EPOXY RESIN COMPOSITES

A Thesis Submitted
In Partial Fulfilment of the Requirements
for the Degree of
MASTER OF TECHNOLOGY

by
SANJAY KUMAR MAZUMDAR

to the


DEPARTMENT OF MECHANICAL ENGINEERING
INDIAN INSTITUTE OF TECHNOLOGY, KANPUR
AUGUST 1988

20 APR 1989
CENTRAL LIBRARY
I. I. T. KANPUR
cc. No. A.104229

ME-1988-M-MAZ-AXI

CERTIFICATE

This is to certify that the thesis entitled, "AXIAL FATIGUE BEHAVIOUR OF KEVLAR FABRIC REINFORCED EPOXY RESIN COMPOSITES" by Sanjay Kumar Mazumdar is a record of the work carried out under my supervision and has not been submitted elsewhere for a degree.


(B. D. Agarwal)

Professor
Mechanical Engineering Department
Indian Institute of Technology
Kanpur - 208016

23 August, 1988

To My
Loving Parents

ACKNOWLEDGMENTS

With profound sense of gratitude, I take this opportunity to put on record my sincere thanks to Prof. B.D.Agarwal for his valuable guidance and encouragement during the course of the present work.

I am grateful to Dr. Prashant Kumar, Dr. N.N.Kishore and Dr. K.Ramesh for their suggestions and interest in my work.

I deeply appreciate the discussions and helpful comments of my friends Bharat Bhushan, K.K.Bajpai, P.Appu Kutten, Mukesh Kumar, M.Mustaq Ahmed, G.K.Adil, D.S.Rajan, M.D.narayanan, T.R.Nayak, A.M.Tarnekar, S.C.Gupta and others with whom I shared many ideas.

I wish to acknowledge the facilities at Experimental Stress Analysis Lab and Material Testing Lab. The assistance of Messers B.K.Jain, S.L.Srivastava, D.K.Sarkar, Sawaran Singh, B.D.Pandey, P.N.Pandey, Arun Shrivastava, A.K.Shukla, Sudhir and Avinash for their dedicated efforts towards several requirements of present work.

A record of appreciation is due to my parents for their efforts in bringing me upto this level.

Finally I wish to thank all those, whose association has made my stay comfortable and enjoyable here at I.I.T.Kanpur.

S.K.Mazumdar

TABLE OF CONTENTS

CHAPTER		PAGE
	ABSTRACT	
1.	INTRODUCTION	1
	1.1 Composite materials	1
	1.2 Fatigue of Composite Material	5
	1.3 Scope of Present Work	11
2.	EXPERIMENTAL PROCEDURE	12
	2.1 Material Used	12
	2.2 Material Fabrication	12
	2.3 Specimen Preparation	16
	2.4 Specimen Design	19
	2.5 Testing Procedure	21
3.	RESULTS ANALYSIS AND DISCUSSION	26
	3.1 Static Behaviour	26
	3.2 Change In Modulus During Fatigue Loading	28
	3.3 Effect Of Thickness Variation	32
	3.4 Damage Model Development	37
	3.5 S - N Curve	46
	3.6 Probability S - N Curve	49
	3.7 Microscopic Study Of Damage During Fatigue Loading	57
4.	CONCLUSIONS AND SCOPE FOR FUTURE WORK	71
	4.1 Conclusions	71
	4.2 Scope For Future Work	73
	REFERENCES	74

ABSTRACT

Investigations have been carried out on Kevlar reinforced epoxy resin composite fabricated by hand layup technique in the laboratory. All tensile static & fatigue tests were performed on an MTS servohydraulic testing machine under load control mode. The loading rate in static test was 0.981 KN/sec and load deflection curve was plotted by X-Y plotter. The fatigue tests were conducted using constant amplitude, tension-tension haversine load cycles with stress ratio equal to 0.1. Frequencies during fatigue cycling were kept low to avoid excessive hysteresis heating of the specimen.

The effect of thickness variation on static strength, load carrying capacity per unit width and fatigue life was found. It has been found during fatigue tests that stiffness of the specimen increases for a considerable no. of cycles. A damage law has been found with fatigue modulus as damage parameter. The S-N curve has been represented by linear law, power law and Hwang-Han relation between normalised fatigue stress and log of fatigue life. The scatter in fatigue data has been analysed by a two parameter Weibull distribution and probability S-N curves have been drawn. The microstructures of damaged fatigue specimens were examined with the help of an Image Analyser to determine the axial fatigue failure sequence and mechanisms.

CHAPTER 1

INTRODUCTION

1.1 COMPOSITE MATERIALS :

A composite is a combined material created by the synthesis of two or more materials - a selected filler or reinforcing agent and a compatible matrix binder (i.e. a resin)- in order to obtain specific characteristics and properties. The components of a composites do not dissolve or otherwise merge completely into each other, but nevertheless do act in concert.

Although the concept of fibre reinforcement is not new, & was even familiar to brickmakers thousands of years ago, the upsurge in the interest in composite materials in the last few decades is due primarily to the high demands on materials performance placed by advanced technologies. Conventional materials are unable to meet these demands.

The application of fiber-reinforced composite materials has been rapidly increased during the past two decades due to its excellent weight saving & load bearing capacity, specially in aircraft & spacecraft areas, which have the typical weight sensitive structures.

The most widely used fibrous composites at the present time are glass-, graphite-, and kevlar- fibre composites. These reinforcing agents are quite diverse with respect to cost, composition, and properties. E-glass fibre composites are most developed and widely used because of its relative low cost. It has a very high tensile strength, but low stiffness. Graphite, Kevlar, and boron (as compared to glass) fibres are most

exceptional because of their high stiffness values, although they are costlier. Of these, the graphite fibres provide a wide range of physical, mechanical and chemical properties. It has high compression strength and a moderate density. It is used in stiffness critical and compression critical uses and the uses where high specific modulus is required. Boron fibres have highest modulus and strength, but also high density. Because of its better high temperature properties it is used in high temperature uses; as in aircraft etc. Because of its highest strength, lowest density and low cost as compared to graphite and boron fibres, Kevlar fibres have become an important reinforcement material today. In the present investigations, Kevlar fibre reinforced composite material is selected.

KEVLAR FIBRE COMPOSITES :

Chemically, the Kevlar Fibres are poly (P-phenylene terephthalamide) [1], which is a poly-condensation product of terephthaloyl chloride and P-phenylene diamine. Kevlar 49 is highly crystalline [2]. The chemical structure of the kevlar fibers is illustrated in Fig.1.1

The rigid linear molecular chains are highly oriented in the fiber-axis direction. Polymer chains are held together in the transverse direction by hydrogen bonding. The difference in bonding (strong covalent bonds in the fiber direction versus weak hydrogen bonds in the transverse direction) is responsible for the anisotropy in the mechanical properties of the Kevlar Fibers; the fibers exhibit high longitudinal strength and low transverse strength.

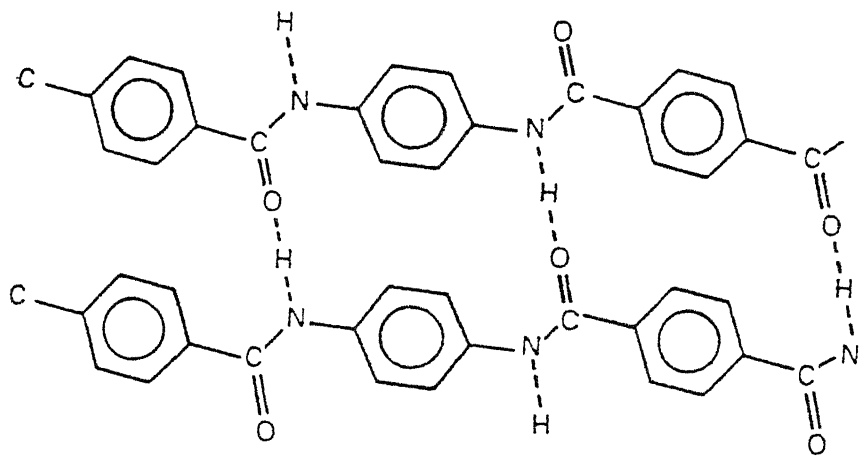


Fig. 1.1 Chemical structure of Kevlar fiber.

The aromatic ring structure of the fiber induces high rigidity and forces extension of the polymer chains (instead of folding), which results in a rod-like structure. This, in turn, gives the fiber a high modulus. The linearity of the polymer chain yields a high packing efficiency, enabling many polymers to be packed into a unit volume. The resulting higher density produces a fiber with higher strength.

The aromatic ring structure also contributes to the chemical stability of the fiber through the delocalization (resonance) of the electrons in the rings. In addition, the high temperature dimensional stability of the Kevlars results from the crystalline nature of the polymer, which is due to the chain rigidity afforded by the aromatic ring structure. Thus, the fiber exhibits no drastic enthalpic changes until it decomposes at a high temperature. This enables the Kevlar fiber to resist temperatures & yet to be less brittle than the cross-linked polymers.

Kevlar fiber composites are used in tension critical structures, ballistic protections and in different high performance composite applications. The wide application of Kevlar fibre composites include the use in rocket engine cases, airplanes components, helicopter blade & other parts, boats, snowmobiles, tracks, offshore structure, pressure vessels, conveyors, ropes & cables. Sporting goods as golf stick etc., helmets, protective gloves, ballistic protective vests etc.

In service, fatigue loads are usually unavoidable. For this reason recent designs do not specify static strength alone as a primary design criterion but also include fatigue analysis.

The demand for improved performance of structural materials in transportation industries, particularly in aircraft, makes fatigue analysis an important consideration. With this view, the fatigue of composite materials has been studied by a large number of investigators. The lack of data available for Kevlar in fatigue, results in selection of its fatigue testing for present investigation.

1.2 FATIGUE BEHAVIOUR OF COMPOSITE MATERIALS :

Machines and structures are often subjected to cyclic loading. It is well known that fatigue strength is smaller than static strength due to the degradation of structure during fatigue cycling. However fatigue behaviour of composite materials is quite different from isotropic materials, such as metal & polymers. Fatigue in metals is understood in terms of nucleation & growth of a single dominant flaw, where as fatigue in composites is characterized by initiation & growth of multiple cracks. Because of the heterogeneity inherent in composites, cracks in composites no longer have the same implications as those in metals. Damage in composites can be any one or several of the following forms: fiber breaks, resin cracks, interfacial debonds, delamination between plies of laminate. All these cracks are not separate but interconnected, making identification of crack paths highly complex. Many of these damage mechanisms occur long before the ultimate failure, and hence , there can be many types of subcritical failures. Each failure should be clearly defined & assessed in its criticality, if engineering designs are to be economical & reliable.

The objectives of fatigue testing (which are more or less common to all materials) are as follows:

1. The understanding of fundamental failure mechanisms leading to material improvement.
2. The determination of the comparative fatigue resistance of materials.
3. The determination of the effect of material composition, processing environment on fatigue properties.
4. The formulation of predictive design rules to allow for stress concentration conditions e.g. mean and alternating stress, complex stress, stress concentrations etc.
5. The conformation of design methods by determining the performance of components.
6. Simulation & assessment of the effect of service loading histories.
7. The assessment of the performance of structures & assemblies.

During fatigue tests, many materials characteristic variables such as residual strength, modulus, compliance, strain, crack length, crack density, number of debonded fibers, etc. may change with number of cycles. As the knowledge and experimental technique are developed, a lot of studies have been performed using the above nature of fatigue phenomena.

Composites have been shown to be more sensitive to strain range as compared to metal [3]. This results in the high cycle fatigue strength of composites being high with respect to static & low cycle fatigue strength. That is, fatigue damage for

composites is more critical in low cycle fatigue region than high cycle fatigue region, whereas for metal fatigue damage may be critical for high cycle fatigue.

Although the tensile strength of unidirectional composites are maximum at a direction of 0° to the fibers, in fatigue the unidirectional construction is not optimum [4]. The best explanation for this phenomenon is the fact that unidirectional material is subjected to splitting & rapid crack propagation in the matrix parallel to the fibre. In general, unwoven materials are superior to woven materials in fatigue because fibres in unwoven materials are straight & parallel and do not get crimped as in the woven fabric construction [5].

A limited work has been conducted on the fatigue behaviour of Kevlar-49/Epoxy composites. Limited fatigue data supplied by the fibre manufacturer and Miner et. al. [6] (Fig. 1.2), shows the fatigue behaviour of Kevlar-49/Epoxy. It can be observed from the figure that Kevlar epoxy & boron epoxy composites display far superior fatigue properties compared to the glass-epoxy composites & Aluminum. Of course, the graphite epoxy composites would be comparable to the Kevlar or boron & are not shown in Fig. 1.2. Hamstad [7] on his work with Kevlar 49/epoxy stands found that at 10 Hz in a sinusoidal mode with applied loads varying from 1-88 % of the strand failure strength, the fatigue life varied from approximately 2000-76,000 cycles. These results clearly illustrate two points : accurate determination of fatigue life requires large numbers of specimens, and as average values for fatigue life is meaningless because there is so much scatter in the lifetime data. Bunsell [8] working on Kevlar-49

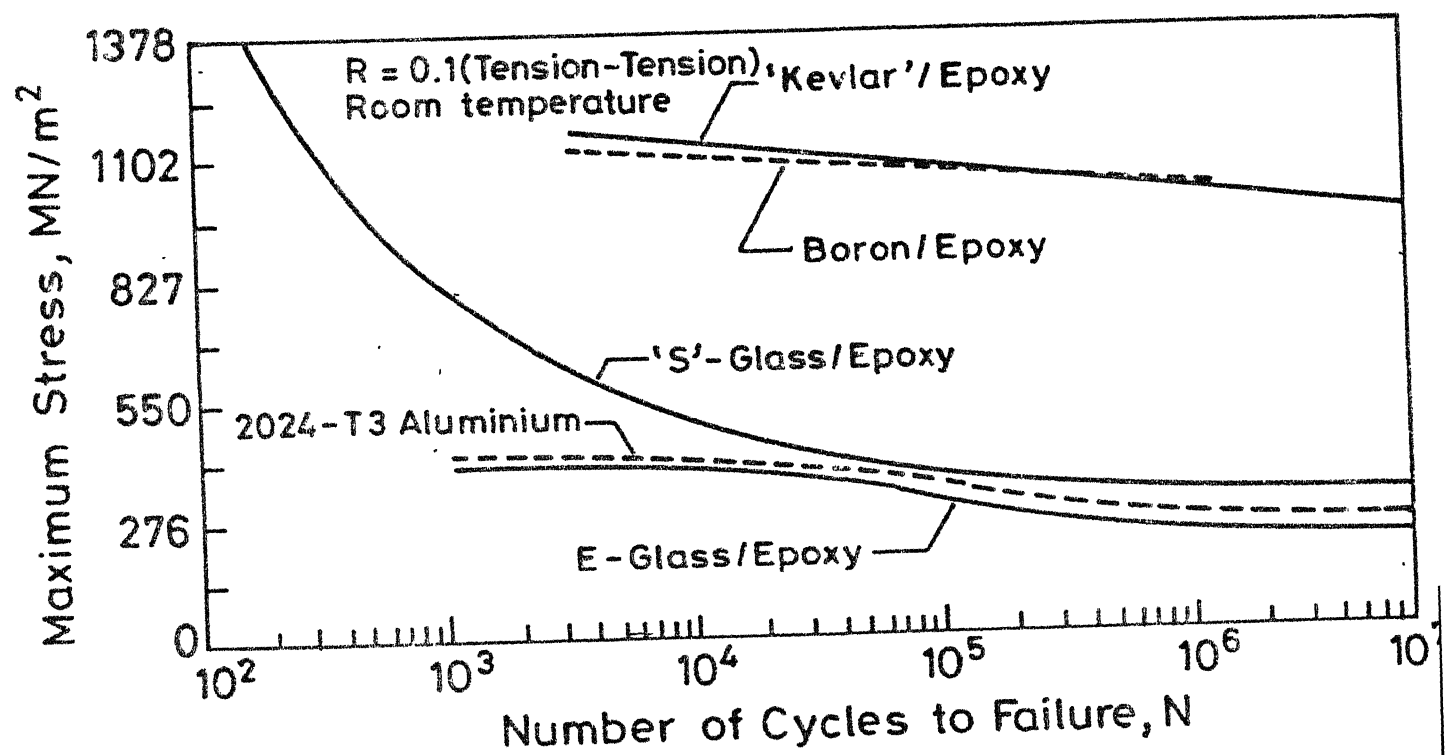


Fig.1.2. Comparison of fatigue characteristics of some unidirectional composites and aluminium.

is considered to have high resistance to fatigue damage as compared to other polymeric fibers. Kevlar does not heat up significantly during fatigue. The effect of stress range at constant maximum load is significant for Kevlar 49 fiber. A definite trend is indicated for increased fiber survival when the minimum load is raised and the maximum load is held constant.

Ganczakowski et. al.[9] found that the stiffness of KFRP unidirectional laminates increases under static loading & with fatigue cycling, although on unloading it may subsequently return to its original value. It has been suggested [8,9] that this increasing stiffness may be due to a re-alignment of both the fibres within a bundle, and the molecular chains within individual fibers. In Kevlar-49 this re-alignment is reversible, but in Kevlar-29 it results in a permanent modulus increase and an associated permanent strain as well.

The character & extent of internal damage have been studied by investigators using different methods. Most of the investigators have used change in structural properties such as static or dynamic modulus [12,13,14,15], residual strength [6,16,17,25], or secant modulus [18] as a measure of internal damage. Hwang & Han [19] defined different cumulative damage models using several physical variables such as fatigue modulus & resultant strain.

The failure of the specimens has been defined by different investigators by different failure criterion. Salkind [3] has suggested that fatigue test data be reported in terms of cycles to a given change in stiffness rather than cycles to fracture.

Many investigators [20,21] have taken the complete separation as the criterion of failure, whereas some [22] were considered a loss of known percentage in stiffness as failure. Sims & Brogdom [23] used Tsai-Hill failure criterion for fatigue tests. Hahn and Kim [18] first stated that failure occurs when the fatigue secant modulus reduces to within the range of static secant modulus. O'Brien et.al.[24] defined a secant modulus failure criterion based on the statement of Hahn & Kim [18]. Hwang & Hahn [19] have given a strain failure criterion.

Fracturographic study has been done by large number of investigators to find out the damage mechanism. Owen & Home [26] quantified fibre debonding & resin crack damage from examination of polished specimen edges. Kim & Ebert [27] have described the failure sequence & mechanism in axial fatigue of GFRP. later they [14] found that the extent & mode of damage is affected by mean and alternating stresses both. James et.al. [28] have studied the effect of convolution of threads in woven cloth reinforced plastics. Owen et.al. [20] have distinguished the debonding, cracking and separation phases in fracture of GRP.

Scatter in the fatigue life data has been analysed by investigators [14,28,29,30]. The data scatter has been represented by many distributions such as normal [29], log normal [14,20] and weibull [18,19,23,25,31,32] distributions. Many investigators [29,31] analysed the fatigue life separately by distributions whereas some other [25,33] developed the models combining the damage model & distribution function, also few others [18,19,23,32] combined the life prediction model with it.

1.3 SCOPE OF PRESENT WORK :

The present investigation has been carried out on Kevlar-49 fabric reinforced epoxy composite laminates. Method of fabrication, specimen preparation and testing details are given in chapter 2. The static and fatigue behaviours of the present material are discussed in sec. 3.1 and 3.2 respectively. The effect of thickness variation on static strength, load carrying capacity/unit width and fatigue life are discussed in sec. 3.3. Analytical model of S-N curve and its statistical analysis is described in sec. 3.5 and 3.6 respectively. Damage accumulation with number of cycles was studied and a damage model was developed with fatigue modulus as damage parameter (sec. 3.4). The microstructures of damaged fatigue specimens were examined with the help of an Image Analyser to determine the axial fatigue failure sequence & mechanisms of Kevlar fabric composites (sec. 3.7). Projecting the highlights of the current investigations, conclusions drawn & scope for future work are indicated in chapter 4.

CHAPTER 2

EXPERIMENTAL PROCEDURE

2.1 MATERIALS USED :

The material selected for the study was Kevlar Fabric reinforced epoxy composite. The specifications of Kevlar-49 and epoxy resin, as supplied by the manufacturers are given in table 2.1 & 2.2 respectively. Although fabric material has lower fatigue properties than unwoven material, it is widely used in practical application due to ease of fabrication. The Kevlar fabric used has unequal counts and denier in cross directions. This makes the fiber volume ratio in warp and fill direction as 10:1 which is generally referred to as the unidirectional weave. All the properties calculated in the present study are for the warp direction which is the dense fiber direction. The fabric used was pretreated by the manufacturer with a coupling agent for epoxy compatibility. Curing times suggested by manufacturer are given in table 2.3. However, the different combinations of curing temperature and time produce no observable difference in properties of the composite.

2.2 MATERIAL FABRICATION :

Composite laminate plates were cast by hand lay-up technique. Twelve layers of fabric was cut to proper size by a special pair of scissors intended for Kevlar cutting. The size of fabric was kept such that a good central portion of 300 x 200 mm² size could be obtained. The fabric was demoiaturised by heating it in an oven at 105°C for the 16 hrs. and cooled in the oven itself to avoid any moisture regain prior to processing.

Table 2.1: Kevlar Fabric Specifications

Product	- Du Pont Co., USA
Category	- Kevlar-49 Fabrics
C.S. Style	- 343
Former Du Pont Style	- 143
Weight (per unit area of fabric), g/m^2	- 190
Tensile strength, N/m	
Warp	- 255700
Fill	- 28700
Count (No. of yarn/in. in warp x fill)	- 100 x 20
Yarn denier (weight in g. of 30,000 ft. long yarn)	
Warp	- 380
Fill	- 195
Weave	- Crowfoot
Finish	- CS - 805
Fiber Properties:	
Specific gravity	- 1.44
Decomposition temp.	- 500°C

Table 2.2 : Epoxy Specifications.

Product	- CIBA Geigy India Ltd.
Category: Resin	- Araldite LY556
Hardener	- Hardner HY951 (10% of Araldite by weight)
Mixing	- At room temperature
Viscosity, cp	- 5000 - 8000
Pot life, hr.	- 0.5 - 1.0
Specific gravity	- 1.2 - 1.3
Tensile strength, MPa	- 55 - 130
Tensile modulus, MPa	- 2800 - 4200
Poisson's ratio	- 0.20 - 0.33
Flexural strength, MPa	- 125
Decomposition temp. °C	- 270 - 280

Table 2.3 : Epoxy Curing Chart.

Curing Temp. (°C)	Curing Time
20	14 - 24 hr.
50	5 - 7 hr.
80	1 - 2 hr.
100	15 - 30 min.
140	5 - 10 min.

About 450 gms of epoxy resin (araldite LY556) was preheated to about 100°C and the temperature maintained for 1 hour to remove absorbed moisture. The resin was then allowed to cool to room temperature (23°C).

Composite plates were cast by hand-lay-up technique between two 25 mm thick M.S. Plates. The M.S. plates were nickel coated on one side and affixed with heating element on the other. A mylar sheet was placed on the lower mould plate. The resin and hardner were thoroughly mixed. The amount of hardner was 10 % of epoxy used. A layer of resin was spread over the mylar sheet and the first Kevlar fabric was placed. Epoxy was applied over the fabric by means of a brush. This process was repeated till all the twelve layers of fabrics were placed. To enhance wetting and impregnation the resin was tapped and dabbed with spatula before spreading resin over fabric pieces. Another mylar sheet was placed over the top most layer. Steel spacers of 3 mm thickness were placed at all four corners between the two mylar sheets. A rubber roller was rolled over the top sheet to squeeze out excess epoxy and entrapped air. The upper mould plate was then placed in position. The mould plates were connected by uniform tightening of nuts on the bolts, provided at the four corners.

The laminate thus prepared was cured for 6 hours at room temperature followed by 12 hours curing at $55-60^{\circ}\text{C}$. The heating was done through several 250 W heating elements placed on the outer surface of each mould plates. The rate of heating could be controlled through a variac. After curing, the composite plate along with mylar sheet was removed. The mylar sheets were then removed to get a fine finished composite plate.

There is no easy method of finding the fiber volume fraction, experimentally for Kevlar fiber composites, because in resin burn-off test, the fibers also burn off[10]. Other methods are tricky, therefore, volume fraction of fibers in the laminate was calculated by knowing the mass of fabric in composite plate as follows:

$$\begin{aligned} V_f &= (A N \rho_{fa} / \rho_f) / (A t) \\ &= N \rho_{fa} / t \rho_f \end{aligned} \quad (2.1)$$

Where,

V_f : Fiber volume fraction

A : Area of the composite laminate

N : Number of fabric layers in the laminate

ρ_{fa} : Areal density of the fabric

ρ_f : Density of fiber

t : Thickness of the laminate

In the present case we have,

$$N = 12$$

$$\rho_{fa} = 0.190 \text{ Kg/m}^2$$

$$\rho_f = 1.44 \times 10^3 \text{ Kg/m}^3$$

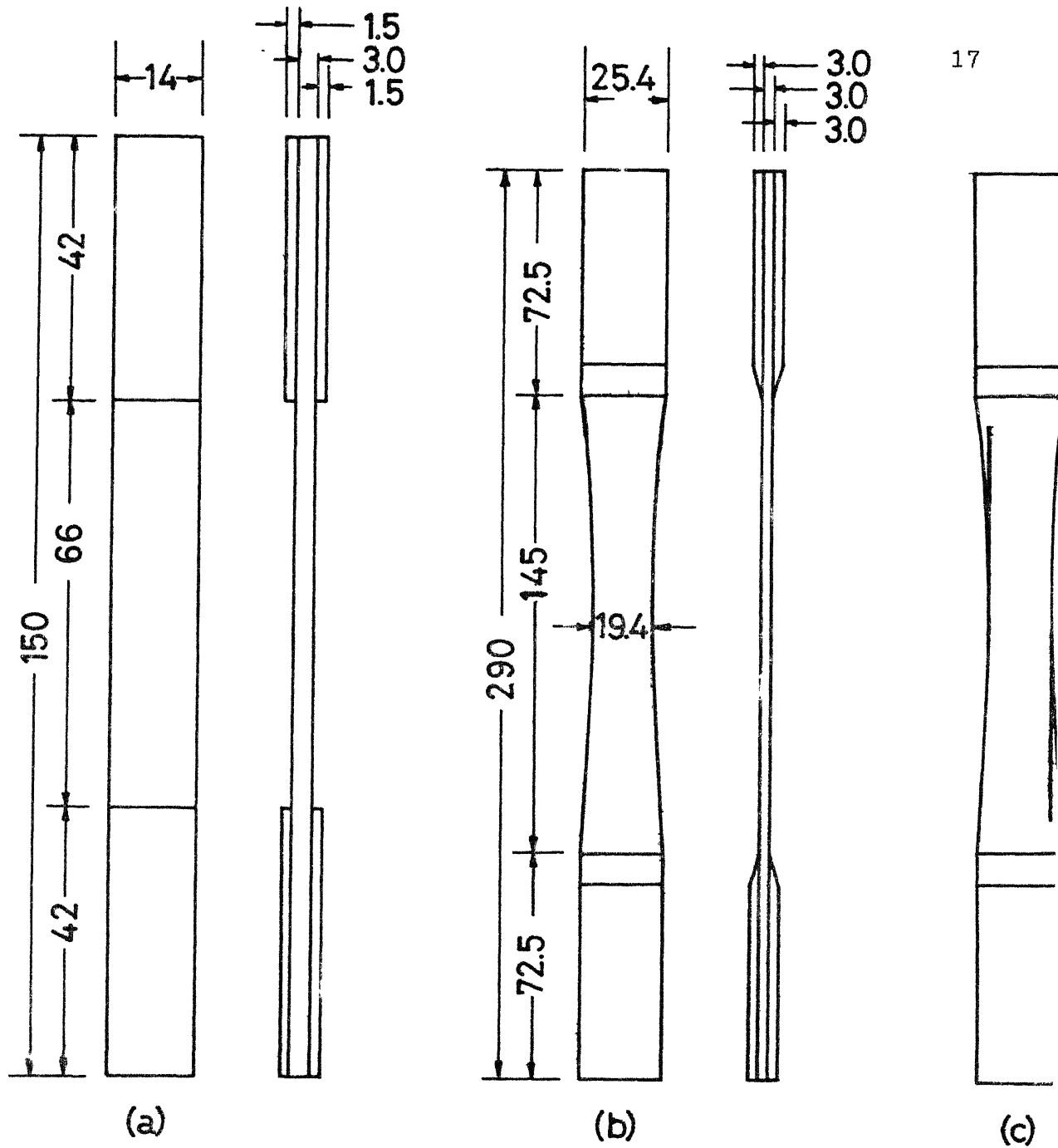
$$t = 3 \times 10^{-3} \text{ m}$$

Hence,

$$V_f = 0.5277 \text{ (52.8 \%)}$$

2.3 SPECIMEN PREPARATION :

Preparation of the test specimens involves cutting the laminates to the desired size, finishing them and then fixing end tabs on them.



All dimensions are in mm

Fig. 2.1 (a) Specimen for present investigation
 (b) Dogbone specimen
 (c) Schematic view of crack formed in dogbone specimen subjected to cycle loading

Rectangular specimen of the dimensions, as shown in Fig. 2.1a were cut from fabricated laminates. The problems encountered during specimen preparation mainly are direct consequences of one of the principal advantages of the aramid fiber such as Kevlar 49, that is its toughness. Test specimens, as well as finished parts, often are fabricated by a variety of machining operations. However, because the aramid fiber is so tough, many of the traditional machining techniques are not suitable. Clements [10] suggested the sectioning of laminates by a fine-grit diamond wheel at low speed. However, by this method the speed of cutting is too slow. Cutting by router at speed of 10,000 and 45,000 RPM produced a lot of brooming at the edge. Cutting with a low power laser beam burns off the edges. These brooming and burning at edges can not be accepted for fatigue tests. Water jet cutters are probably the best but are not available in the laboratory.

The best results in cutting laminates were obtained through a circular saw when unconventional side (slant side of teeth) of a metal slitting fine toothed H.S.S. cutter was used at high speeds [33]. Cutter size used is 6 inch dia. and .08 inch thickness with 7-8 teeth per inch. Fine toothed cutter would be better. Circumferencial speed of the cutter was about 30 m/s. Water was used as coolant. With this setup, cutting speed in the dense fiber direction (cutting less fibers) was quite high and in cross direction it was moderate. The quality of the edge was quite good except few broomed fibers at one side of edge from which cutter comes out after cutting. This brooming was easily removed by abrading the edges on simple wood sand papers and good

edge finished was obtained.

For preparing dogbone specimens, rectangular blanks of 290 x 25.4 mm² were first cut by circular saw. These blanks were then machined to the shape (Fig. 2.1b) by using an aluminium template and a diamond impregnated router. The edges were then abraded to get fine surface finish.

Material selected for end tabs was glass fabric reinforced epoxy. Laminates for tab was made with 8 layers of glass fabric reinforced with epoxy by hand-lay-up technique in the laboratory. The thickness of the tabs was kept 1.5 mm and was cut to the shape of 42 x 14 mm² by circular saw. The adhesive used for affixing end tabs to the test pieces was epoxy. At a time six test pieces were affixed with tabs in a drill press vice as shown in Fig. 2.1. and curing was done for 24 Hrs at room temperature. To avoid sticking of two adjacent tabs mylar sheet was inserted in between two tabs. During design of specimen tapered end tabs with different tapered angle and different thickness were used as a trial. Tapering of end tabs was done with the help of grinding wheel. Initially, C-clamps were used for applying pressure on end tabs during curing. Later, a drill press vice was used to give uniform pressure on end tab surface during curing. Moreover it helped in affixing end tabs in more number of test pieces at a time.

2.4 SPECIMEN DESIGN :

The most frustrating testing problem with the aramid/epoxy composites had been the debonding of the end tabs before the failure of end tabbed longitudinal tensile specimens [10]. This

apparently results from the low strength of the composite/adhesive interface.

A careful attention was paid to the design of the specimen for static and fatigue tests. Firstly, rectangular and then dogbone specimens of different sizes and shapes were used without end tabs. In all the cases shear failure of specimen took place at the grip much before the failure of specimen, due to the small shear-to-axial-strength ratio of composite. To avoid the damage in the outer layer, end tabs of different thickness with different tapered angle were used. Perspex and different glass/epoxy composites were used as tab materials and epoxy as adhesive. In these cases debonding of end tabs took place before the failure of the composite material itself. Debonding of tapered end tabs was initiated at the end of tapered surface. This apparently results from the low strength of composite/adhesive interface.

Nearabout 20 dogbone specimens of the size shown in Fig. 2.1b were used for static tensile and fatigue tests. During uniaxial tensile test, specimen did not fail exactly at the middle of gauge length but failure took place some where in between gauge length. The problem encountered during fatigue tests of dogbone specimens was, the formation of a crack parallel to the loading direction (tangent to the curved edge) along the longitudinal axis of specimen which propagated towards the grip. Final specimen failure took place near the grip. This splitting resulted from low shear-to-axial-strength ratio of composite. The crack growth tangential to neck is schematically shown in

Fig. 2.1c. It was observed during fatigue cycling that the outer layer of specimen got damaged due to friction between tab and specimen at the debonded region and this resulted in separation of outer layers from inner layers. Due to the splitting of specimen tangential to the neck, dogbone specimen was rejected.

After several trials, rectangular specimens of length 150 mm & width 14 mm were selected with rectangular end tabs of length 40 mm & thickness 1.5 mm for static & fatigue tests as shown in Fig 2.1a. The material used for tab was glass fabric/epoxy composite, with epoxy as adhesive. The specimen finally selected gave good results and failure of specimen took place in the gage section without debonding of end tabs.

2.4 TESTING PROCEDURE :

Whenever new materials are made available, engineers will naturally require fatigue properties if they are to be used under the condition of varying load or deformation. Initially simple comparative data are required, followed up with more specific design data & information on the effect of environment, manufacturing methods, etc. Finally as more demanding applications are fulfilled, test data on component and structures are required. The design engineers attitude to a new material must largely be that it is one more material in the stock from which selection can be made to produce efficient and economic designs. It is helpful if all available data and related design techniques are as far as possible similar in nature. Thus it seems desirable to use test methods for fatigue testing of FRP which are related to those for metals as closely as possible.

For the present investigations, all the tests were performed at room temperature (23°C). All tensile static and fatigue tests were conducted on an MTS servohydraulic testing machine (Fig. 2.2) under load control. The testing machine has the capacity of ± 10 tonne which can be applied in the form of a sine, haversine, ramp, haversine square, invert.

For static tests, the specimen was secured between the grips. A small try square was used to align the specimen in vertical direction. The grip was of wedge shape with serrated surface for holding the specimen. Load was applied at the rate of 0.981 kN/sec & at the same time load-deflection curve was plotted using the X-Y recorder. Ultimate tensile load was noted from digital indicator.

All fatigue tests were performed in tension-tension mode with stress ratio R equal to 0.1 . Nearabout 65 specimens were tested. Maximum stress (S_{max}) in fatigue cycles was 90, 85, 80, 70, 65, 60 and 50 percent, respectively, of the average ultimate static strength. These stress levels were selected so as to vary the fatigue life from hundred cycles to half million cycles. For 90% and 85% stress levels, frequency was kept at 1 Hz while for 80%, 70% and 65% stress levels, frequency was gradually & slowly increased to 3 Hz and for 60% & 50% stress levels frequency was raised slowly to 6 Hz.

For testing, specimen was secured between the grips and was kept in vertical position with the help of a small try square. The same holding device was used as in the static test. Then, the stroke value was brought to zero position for zero load on the specimen & the X-Y recorder was switched on and positioned

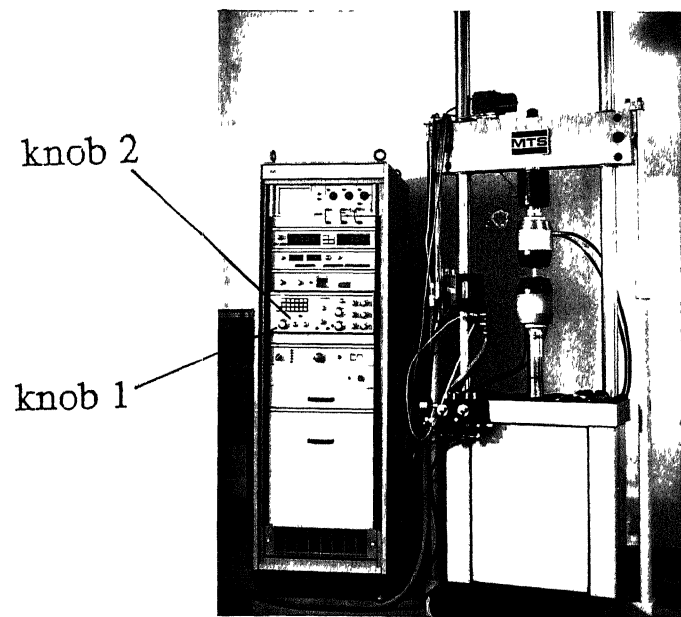


Fig. 2.2 An overall view of MTS testing machine
with specimen under test.

on the graph paper. Operating in the load control mode, a tensile load of P_{min} corresponding to the minimum stress in fatigue cycling denoted by S_{min} was applied with the help of Knob 1 & $P_{max}-P_{min}$ was fixed using Knob 2; P_{max} being the load corresponding to the maximum stress denoted by S_{max} . A haversine load cycling in the range of P_{min} to P_{max} was then started. For the first 5 cycles a frequency of 0.1 Hz was used and a load-deflection graph was plotted. Subsequently the machine was run at 1 Hz then the frequency was increased as described for different stress level (as explained earlier in this section). After 25 cycles the loading was rechecked from the digital indicator to make sure that the loading remains in the range of P_{min} & P_{max} . Periodically loading was checked from the digital indicator. The specimen was run till the occurrence of failure and fatigue life was recorded in cycles from the counter. During fatigue cycling upper and lower stroke values (δ_{max} & δ_{min}) corresponding to P_{max} and P_{min} were noted at fixed intervals from the digital indicator. These readings were used to calculate the average modulus at fixed intervals from relation;

$$E = \frac{S_{max} - S_{min}}{(\delta_{max} - \delta_{min}) / l} \quad (2.2)$$

Where,

E : Average modulus at a specific cycles

S_{max} : Maximum stress applied during fatigue loading.

S_{min} : Minimum stress applied during fatigue loading.

δ_{max} : Maximum stroke value corresponding to S_{max} at a specific cycle.

δ_{min} : Minimum stroke value corresponding to S_{min} at a specific

cycle.

l : Gauge length of the specimen.

DAMAGE STUDY:

The development of damage was monitored microscopically by polishing one edge of the specimen before testing. The polishing was carried out by conventional metallographic techniques taking care not to overpolish and tolerating some scratches in the matrix. The final stage of the polishing was carried out using rotary polisher covered with velvet cloth. Water mixed with alumina powder was used as the abrasive during polishing. After that, the specimen was washed with water and then dried using on air blower. Then specimens were marked at three places; One at middle and two was either side of middle marked near to grips. These three marked places were taken as representative sites for microscopic examination. For the present investigation, microscopic examination was done with the help of an image analyser. Representative sites were photographed before loading & after fixed intervals of fatigue cycling. Some photographs of the surface of the specimen were taken to analyze the damage on the surface. Photographs were taken using automatic camera fixed in the microscope.

CHAPTER 3

RESULTS, ANALYSIS AND DISCUSSION

Fatigue of Kevlar-49 fabric/epoxy composite has been studied. The composite plates made in the laboratory had about 52% fibers by volume. The straight sided specimens with end tabs were 150 mm long and 14 mm wide.

Static tension and fatigue tests were conducted in an MTS servohydraulic test machine. Damage in terms of matrix cracking, debonding and fiber breaking during fatigue cycling was studied with the help of an image analyser. For this purpose one edge of the specimen was polished for microscopic examination.

3.1 STATIC BEHAVIOUR:

Static behaviour of Kevlar/epoxy composite was studied through tension tests on 34 specimens. The tests were conducted under load control with a loading rate of 0.981 kN/Sec. An extensometer of gauge length 25 mm was used to measure the strain which was directly plotted against stress with the help of an X-Y recorder.

A typical stress-strain curve is shown in Fig. 3.1. Stress-strain curve is linear upto failure. Following are the average static properties of the composite:

Ultimate tensile strength	: 1024.4 MPa
Elastic modulus	: 50.7 GPa
Ultimate strain to failure	: 2.02 %
Poisson ratio ν_{LT}	: 0.19

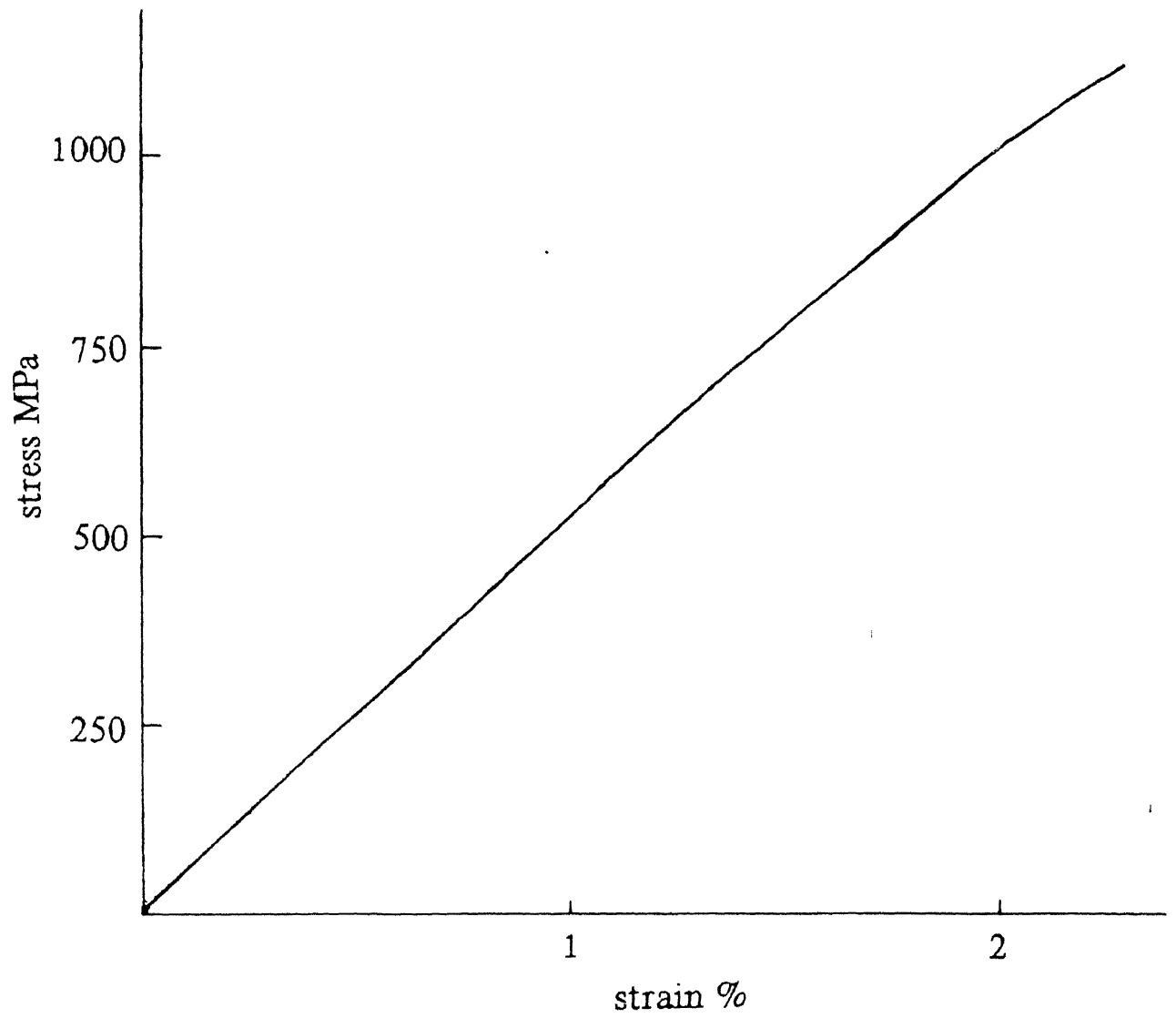


Fig. 3.1 Typical stress-strain curve in tensile test.

3.2 CHANGE IN MODULUS DURING FATIGUE LOADING :

All fatigue tests were also conducted on an MTS servohydraulic testing machine under load control mode at room temperature (23°C). The specimens were cycled between fixed stress limits with a tension-tension haversine load cycle and a stress ratio $R = 0.1$. The maximum stress was kept at 90, 85, 80, 70, 65 and 60 percent of the average static ultimate failure stress so that fatigue life of specimens varied between 100 to 5×10^5 cycles. At least 10 specimens were tested at each of these stress levels. Three specimens were tested at a maximum stress of 50% and one at 40% of ultimate tensile strength.

During fatigue tests, maximum and minimum stroke values corresponding to maximum and minimum load were noted from the digital indicator, at certain intervals. These stroke values were used to determine average modulus at intermediate cycles. The average value of modulus is calculated from relation :

$$E = \frac{S_{\max} - S_{\min}}{(\delta_{\max} - \delta_{\min}) / l} \quad (3.1)$$

Where,

E : Average modulus at a specific cycle,

S_{\max} : Maximum stress applied during the fatigue cycle,

S_{\min} : Minimum stress applied during the fatigue cycle,

δ_{\max} : Maximum stroke value corresponding to S_{\max} at a specific cycle,

δ_{\min} : Minimum stroke value corresponding to S_{\min} at a specific cycle,

l : Specimen gauge length.

A typical stress-strain curve for the first few fatigue

cycles is shown in Fig. 3.2. An extensometer of gauge length 25 mm was used to measure the strain which was directly plotted against stress with the help of an X-Y recorder.

When a composite material is subjected to fatigue cycling, it undergoes degradation in the form of matrix cracking, debonding, fiber breaking, delamination and combinations of these. Therefore it can be expected that its modulus will decrease. Variation of modulus with number of cycles has been found for all the specimens for 90%, 80% and 70%, stress levels. A typical variation in modulus at 90%, 80% and 70% stress levels is plotted in Fig. 3.3. taking normalized modulus (E/E_0) as ordinate and log (no. of cycles) as abscissa. It is clear from the figure that the normalized modulus for all the stress levels increases with increase in no. of cycles. The average increase in modulus for all the cases was found to be 5% of initial modulus (E_0). In 90% stress level failure of specimen takes place suddenly without decrease in modulus. In 80% and 70% stress levels modulus of composite decreases during final stage of the test. Obviously this is in contradiction to logical expectations. However, it can be explained as follows : It has been reported that the modulus of Kevlar-49 fibres increase with fatigue cycling [8,9]. This increase in modulus has been attributed to a re-alignment of both the fibers within the bundle as well as the molecular chains within the individual fibers [8,9]. In the case of present KFRP composite, this increase in modulus is counter acted by a decrease in the modulus due to degradation of the material in the form of matrix cracking, debonding, fiber breaking and delamination. The net effect is that the modulus of

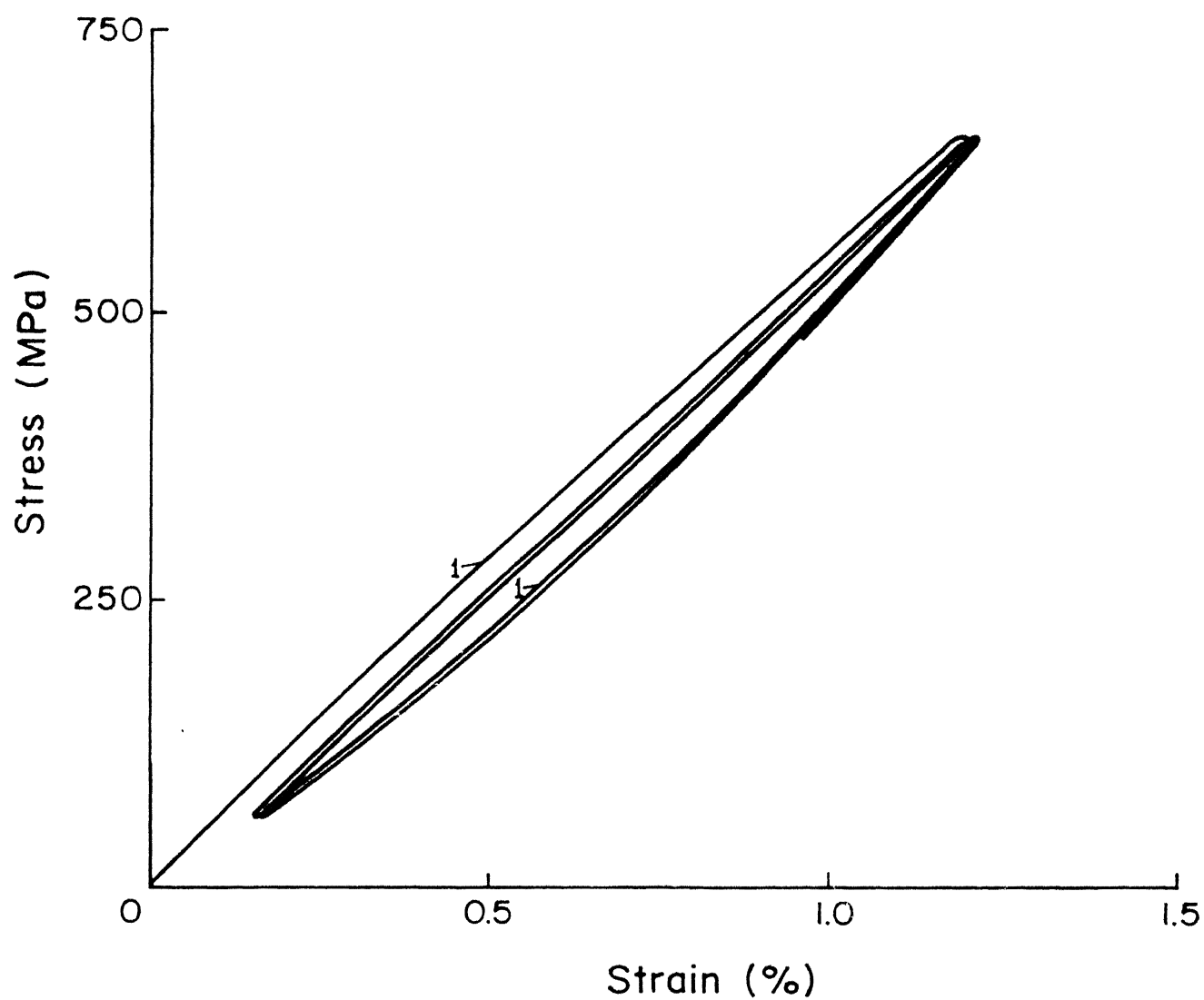


Fig. 3.2 Typical stress-strain curve in cyclic loading at low frequency (0.01 Hz)

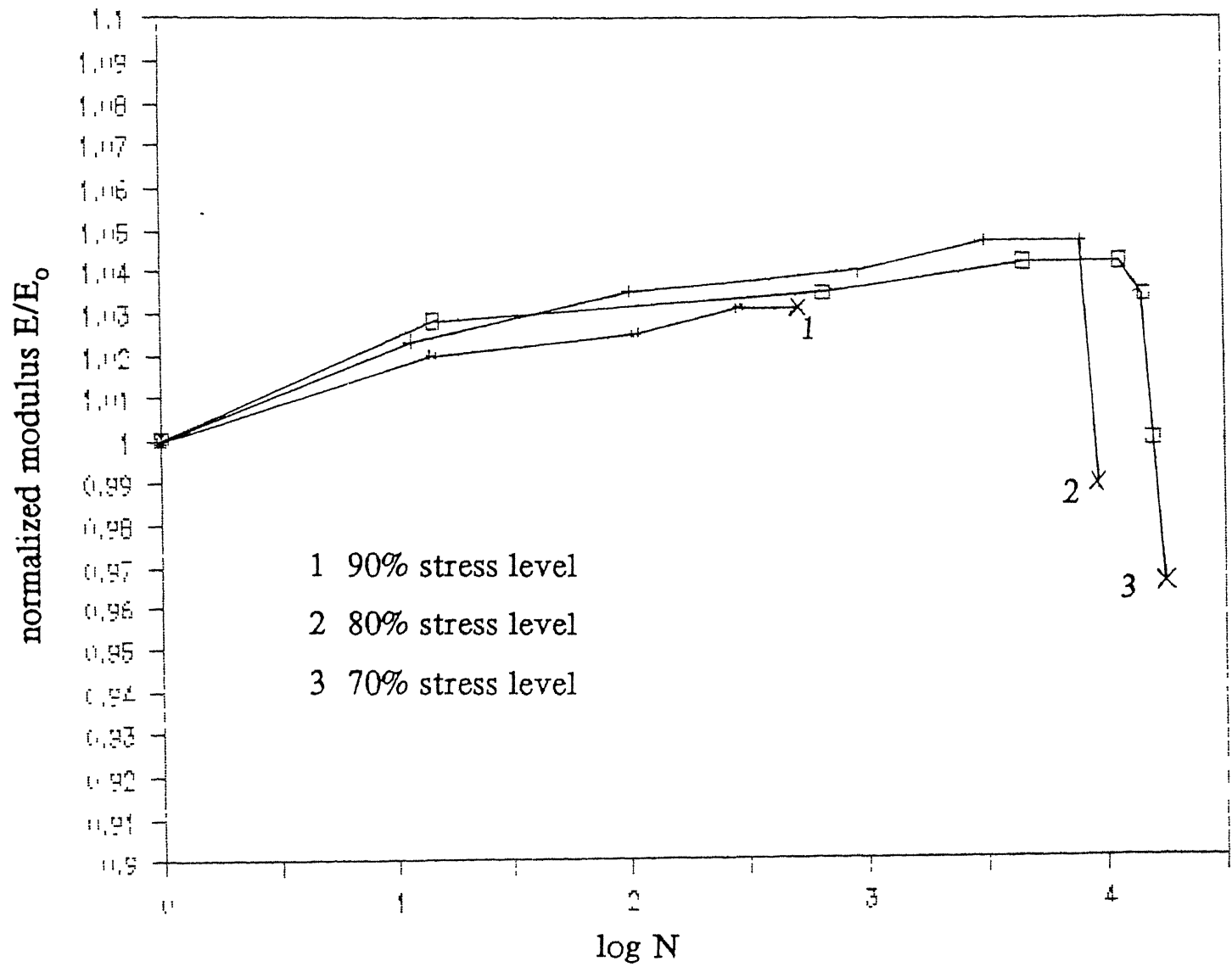


Fig. 3.3 Variation of modulus during fatigue cycling.

the KFRP composite material increases upto a stage where the degradation of the materials is not substantial. The decrease in modulus during final stage of 80% and 70% is probably due to the dominance of the effect of degradation of the material.

To study the nature of increase in modulus, fatigue cycling of two or three specimens at each of these stress levels was stopped, the specimens unloaded and allowed to relax freely for a period between 30 minutes to 300 hrs. The specimens were then cycled again. Fatigue tests on each of these specimens were interrupted several times until 80% of their expected fatigue life. It was found that increased modulus reverts back to its initial value when the specimen is allowed to relax freely for 48 hrs. Similar behaviour has been reported by other investigators also [9]. Some specimens were unloaded to zero load but left in the testing machine and the machine switched off. For such specimens the stress-strain curve does not revert back to its initial stress-strain curve. This is due to the fact that, the specimen was not free to relax i.e. contraction of specimen was not allowed.

From the above results, it appears that the temporary increase in strain produced during fatigue cycling is dissipated by some time dependent behaviour when the laminate is allowed sufficient time to relax freely. Ganczakowski et.al. [9] have suggested that it may be possible to model this behaviour by a 'spring and dashpot' arrangement.

3.3 EFFECT OF THICKNESS VARIATION :

All the composite plates were fabricated by hand-lay-up

technique with 12 layers of Kevlar fabric. It was found that the cured thickness varied from plate to plate depending on the amount of resin squeezed out. The variation in thickness from specimen to specimen was in the range of 2.96 to 3.5 mm.

Static tests were conducted on 35 specimens and the ultimate tensile load was found out in each case. The load carrying capacity per unit width of the specimen is plotted against thickness in Fig. 3.4. It is clear from the figure that the effect of thickness variation on the load carrying capacity per unit width is insignificant.

A composite material mainly derives its strength from the fibers, and all the specimens contain the same no. of fabric layers, it can be expected that the ultimate tensile load will be nearly same for all the specimens. This prediction has been supported by experimental results which are plotted in Fig. 3.4 with thickness as the abscissa and load carrying capacity per unit width as the ordinate.

The effect of thickness on static strength is shown in Fig. 3.5. The test data in Fig. 3.5 conform to the following best fit linear equation :

$$S_u = 1800.71 - 2438.83t \quad (3.2)$$

Where,

S_u : Ultimate tensile strength of the specimen in MN/m^2

t : Thickness of the specimen in cm.

The coefficient of correlation r for the test data is 0.8387. it is clear from the figure that the strength decreases as thickness increases. The reason is that the tensile strength

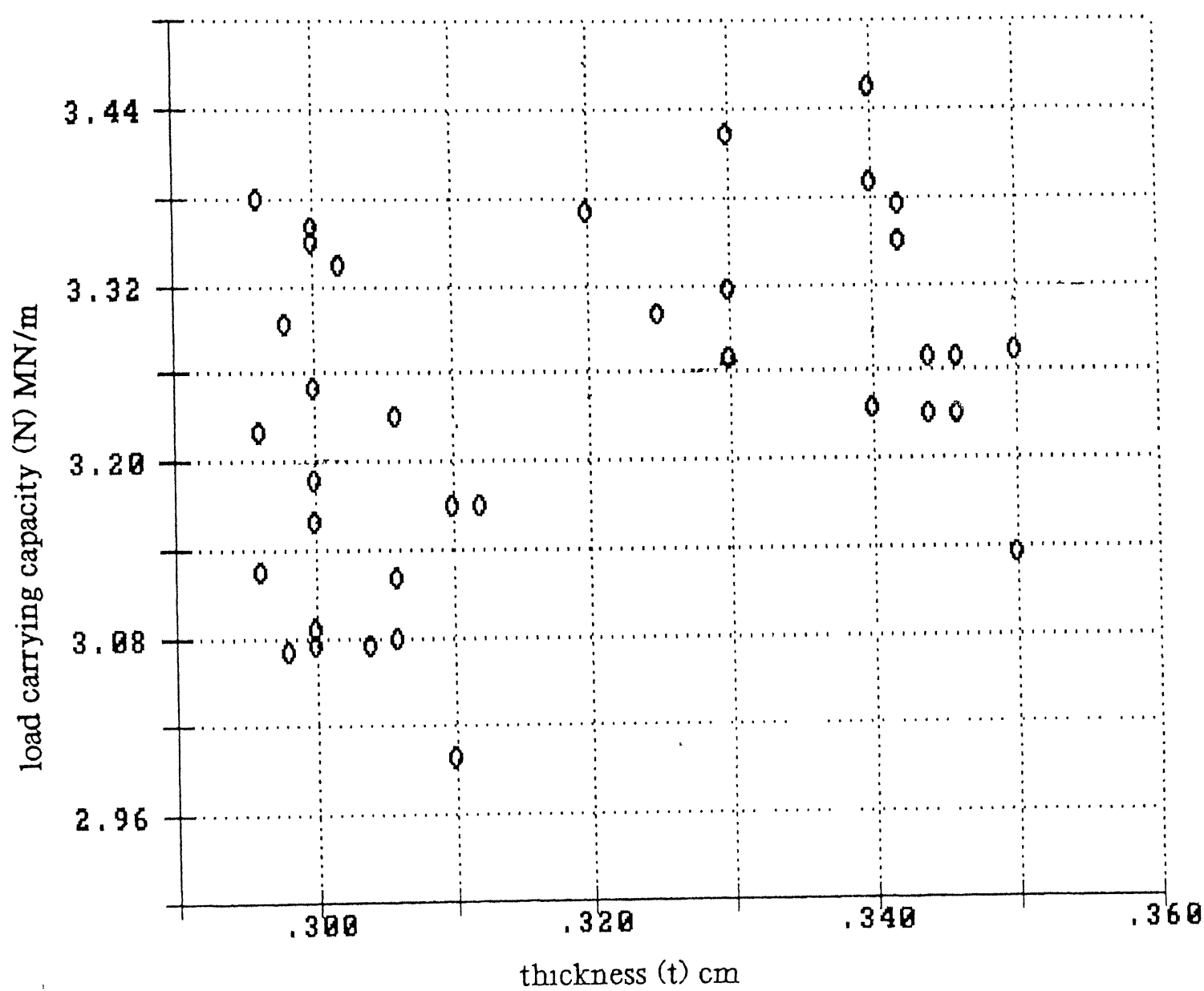


Fig. 3.4 Effect of thickness on load carrying capacity / unit width.

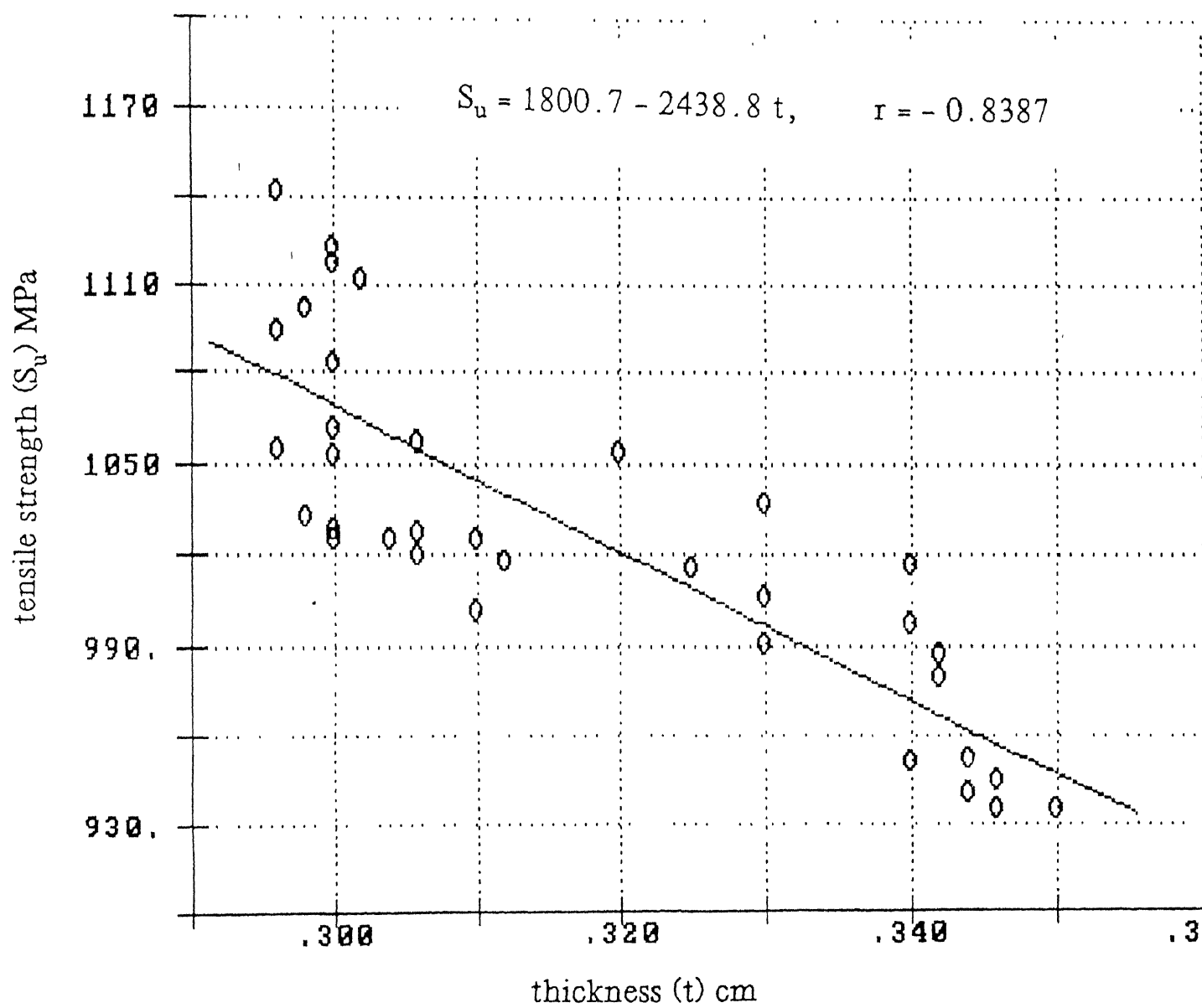
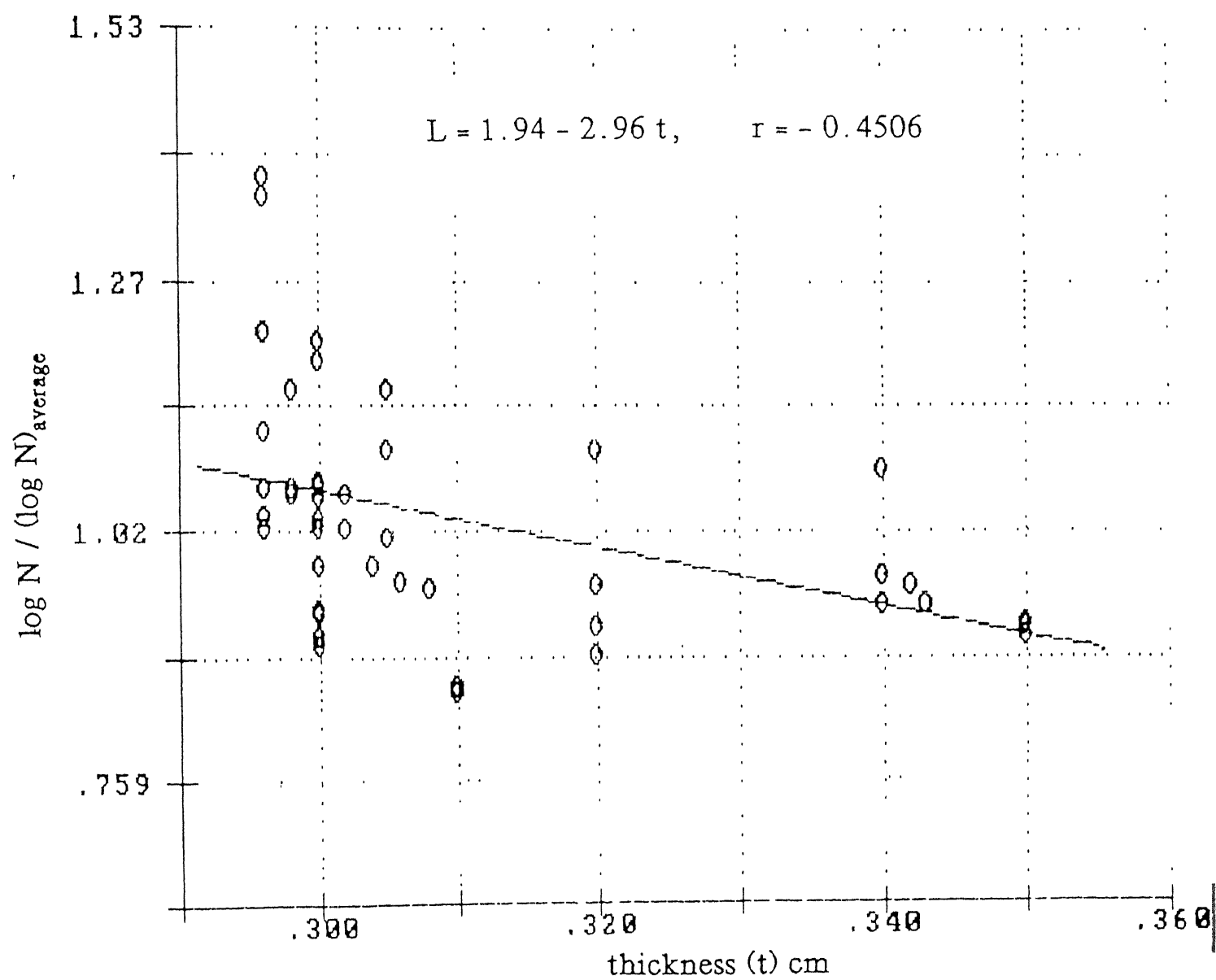


Fig. 3.5 Effect of thickness on static strength.



is inversely proportional to the cross sectional area of the specimen. The effect of thickness on ultimate tensile load is found to be insignificant as shown in Fig.3.4. Therefore, if the width of the specimen is maintained constant, strength increases with decreasing thickness.

The effect of thickness variation on fatigue life is shown in Fig. 3.6 by plotting $\log N_f / (\log N_f)_{av}$ against thickness. The test data of Fig. 3.6 was fitted to a linear equation of the form :

$$L = 1.94 - 2.96t \quad (3.3)$$

Where,

L : $\log N_f / (\log N_f)_{av}$.

t : thickness of specimen in cm.

N_f : fatigue life of the specimen.

The coefficient of correlation for the test data is 0.4506. The trend given by the above equation is not reliable because coefficient of correlation is low (0.4506). This figure shows that the effect of thickness on fatigue life is insignificant. This is expected because the no. of fabric layers is same for each specimen.

3.4 DAMAGE MODEL DEVELOPMENT :

Defining fatigue damage of composite materials is not a simple problem. Failure modes of composite materials are complex and quite different from those of isotropic materials. For short fiber composite materials, fiber matrix debonding, fiber fracture, and matrix failure are the main possible failure modes. For composite laminates, delamination is also a possible failure

mode, in addition to the above failure modes. Based on these failure modes, crack length, crack density, delamination, and no. of debonded fibers are apparent damage mechanisms, which can be detected through microscopes or NDT instruments. These variables could be used to characterize the damage. Besides the above visible physical variables, modulus, acoustic emission, residual strength, and strain, which would vary during fatigue loading, may be used to characterize damage. Some investigators [16,21] studied the progressive nature of damage qualitatively where as many others [12,19,26,32,34] studied it quantitatively and developed the different damage models to predict damage accumulation during fatigue. Hwang & Han [19] proposed some damage models using fatigue modulus [15] and resultant strain as damage parameters.

It is apparent from the study of modulus during fatigue loading [Sec.3.2] that young's modulus is not particularly a good damage parameter for KFRP, especially in fatigue loading [9]. For the present study, complete separation of the specimen is taken as the failure criterion and the fatigue modulus is taken as the damage parameter which decreases continuously, with fatigue cycling. Fatigue modulus is defined as the slope of the plot of applied stress vs. resultant strain at a specific cycle. Fig. 3.7 shows schematic diagram of stress-strain curve during cyclic loading. Due to the degradation of composite materials, stress-strain curve changes as the material is cycled continuously. In Fig. 3.7 fatigue modulus $F(n)$ at N^{th} cycle is represented by the slope of the line AN between applied stress and resultant strain at N^{th} cycle.

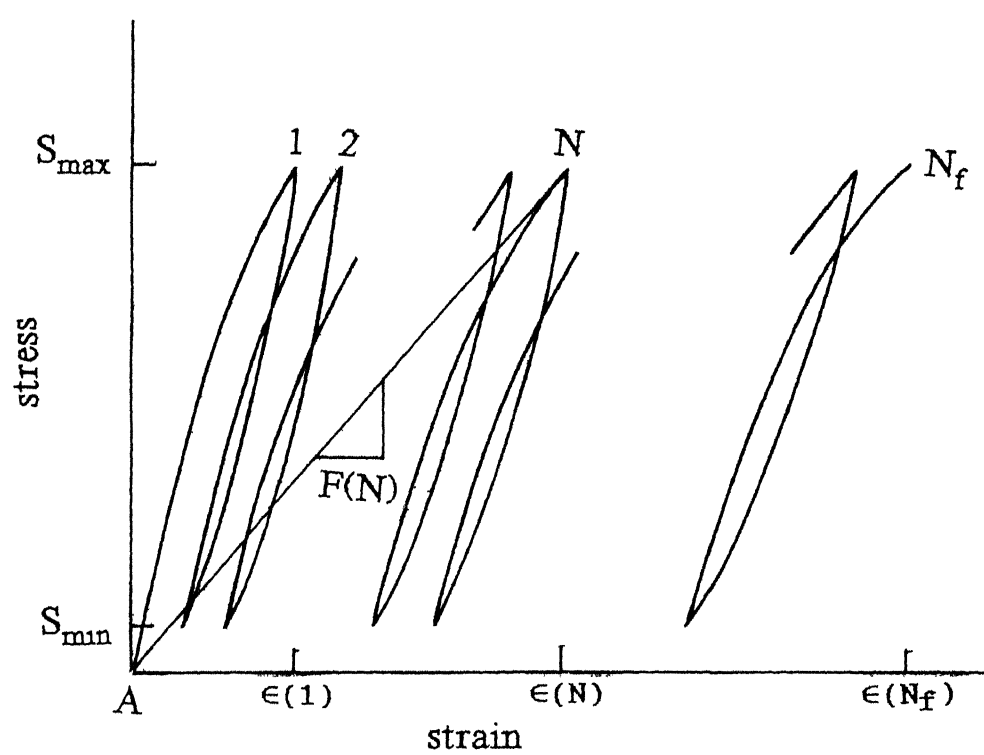


Fig. 3.7 Schematic representation of fatigue modulus.

Therefore,

$$F(N) = S_{\max} / \epsilon(N) = S_{\max} / \delta_{\max}(N)/l \quad (3.4)$$

Where,

$F(N)$: Fatigue modulus at N^{th} loading cycle,

$\epsilon(N)$: Resultant strain at N^{th} loading cycle,

S_{\max} : Maximum applied stress,

$\delta_{\max}(N)$: Stroke value corresponding to S_{\max} at N^{th} loading cycle,

l : Specimen gauge length.

Most of the damage models proposed in the literature required the damage and the number of cycles to be normalized in order to make the model simple. Thus the fatigue modulus has been normalized with respect to the difference in maximum fatigue modulus and minimum fatigue modulus. Maximum fatigue modulus occurs at first cycle and minimum fatigue modulus occurs at failure. Normalizations have been done so that both the normalized quantities varies from 0 to 1. The normalized fatigue modulus is referred to as normalized damage in the present study.

Normalized damage,

$$D = \frac{F(1) - F(N)}{F(1) - F(N_f)} \quad (3.5)$$

Where,

$F(N)$: The fatigue modulus at N^{th} number of cycles,

N_f : Number of cycles to failure, i.e. fatigue life.

Normalized number of cycle,

$$N_{\text{nor}} = \frac{N - 1}{N_f - 1} \quad (3.6)$$

The normalized damage has been plotted against the normalized number of cycles for maximum stress levels at 90, 80, 70, 60 percent, respectively of the average ultimate failure stress obtained from static test.

It has been observed that the model formulated by Agarwal & Bhushan [35] fits well with the findings of the authors. The model with slight rearrangement of constants can be written as,

$$D = A \left(1 - \frac{e^{c_1(1-N_{nor})} - 1}{e^{c_1} - 1} \right) + (1 - A) \left(\frac{e^{c_2 N_{nor}} - 1}{e^{c_2} - 1} \right) \quad \dots (3.7)$$

Where,

c_1, c_2 : constants,

A : Weighing constant.

The constants were determined by fitting the model to the experimental points by minimizing variance using Powel's method.

The model is fitted for 90, 80, 70, 60% stress levels separately and shown in Fig. 3.8 to 3.11 along with the experimental points.

The values of the constants for each of the damage curves are mentioned in figures. The slopes of these curves are referred to as the damage rates. These curves can be discussed in terms of three well defined stages, namely the damage initiation stage (stage I), steady damage stage (stage II) and the damage propagation stage (stage III). Following an initial rapid damage rate, the damage rate decreases with number of cycles in stage I. In stage II the damage rate reaches to steady state in which the damage rate changes little with the number of

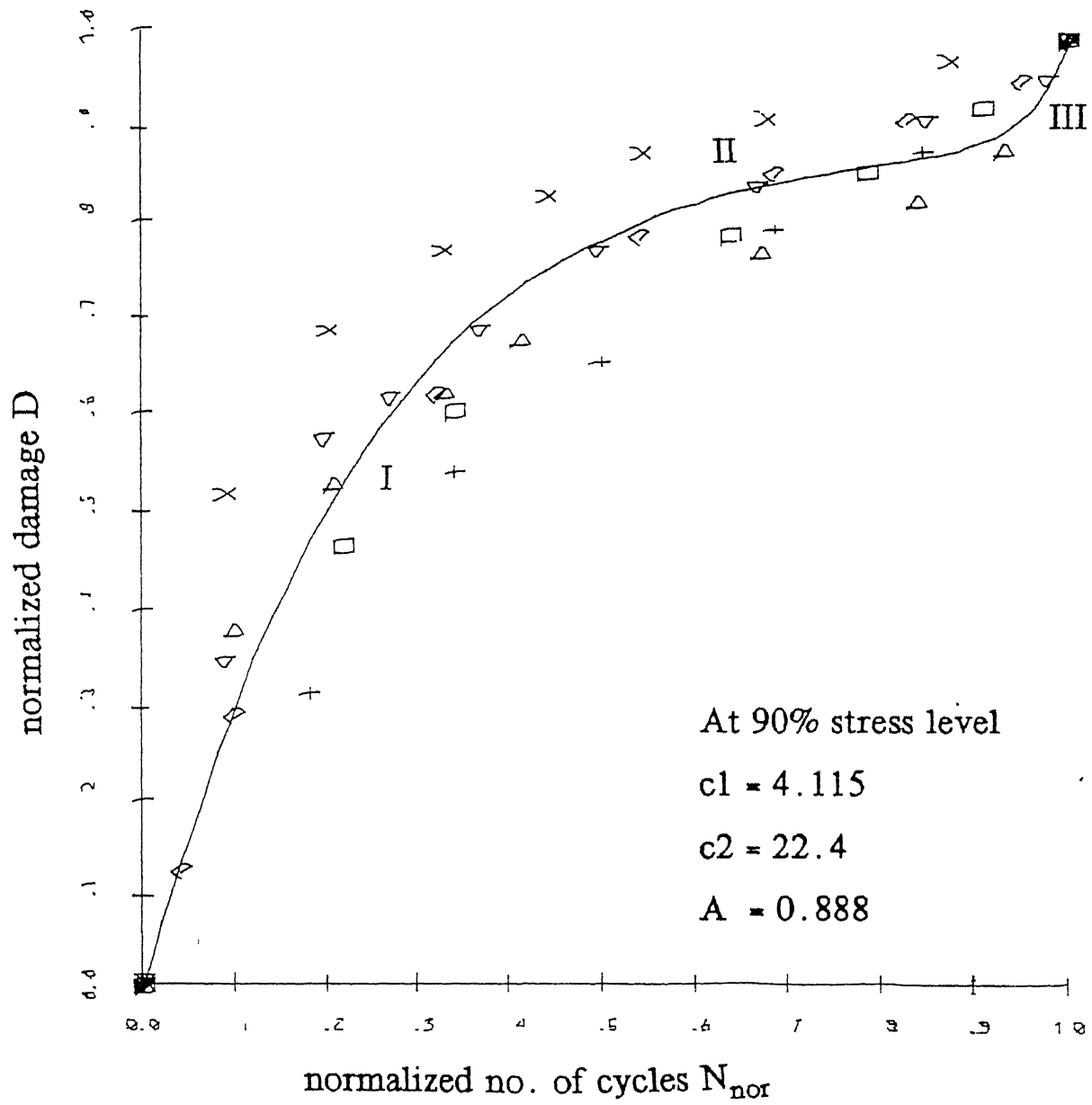


Fig. 3.8 Damage accumulation plots (each symbol represents a specimen)

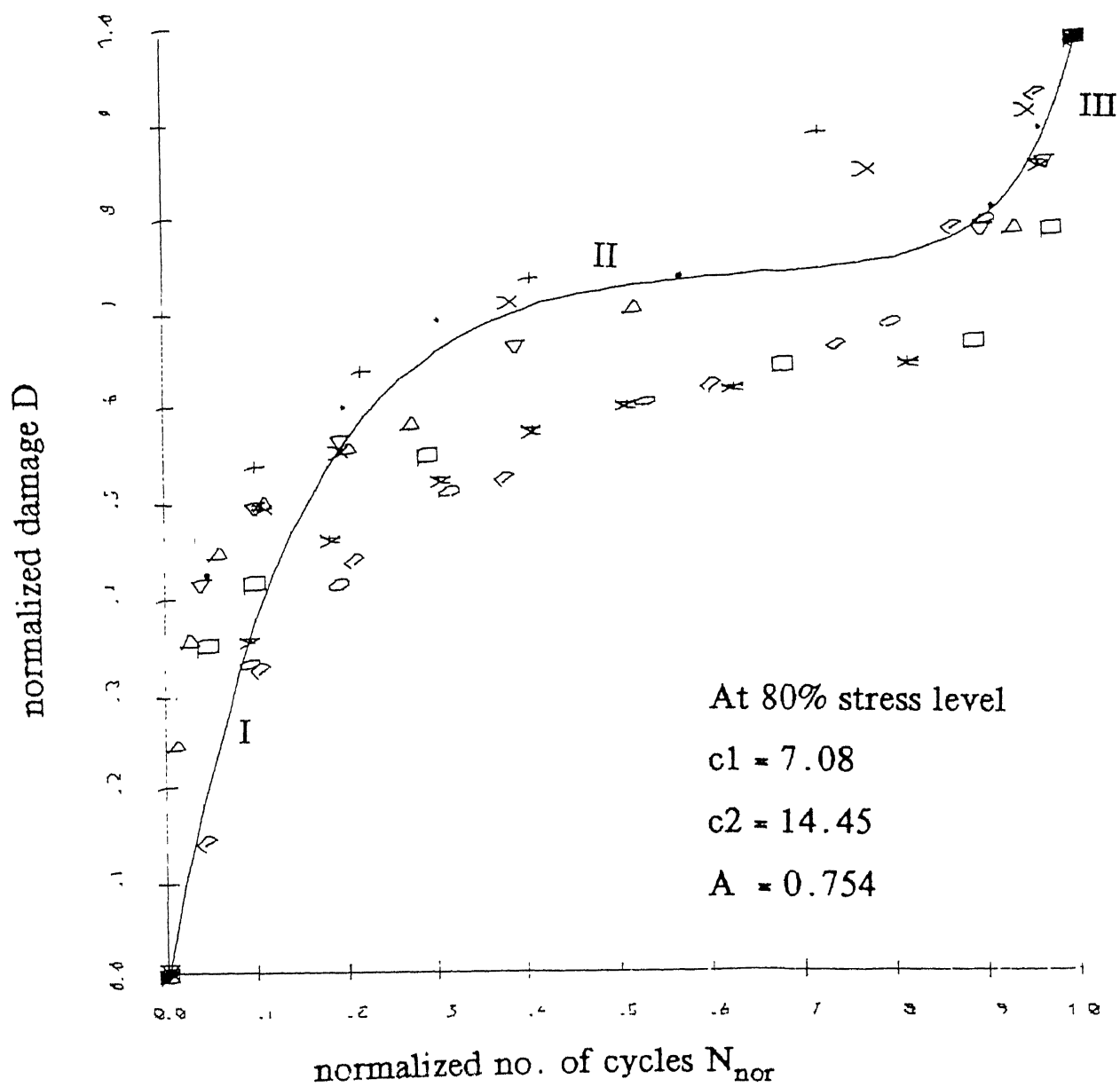


Fig. 3.9 Damage accumulation plots (each symbol represents a specimen)

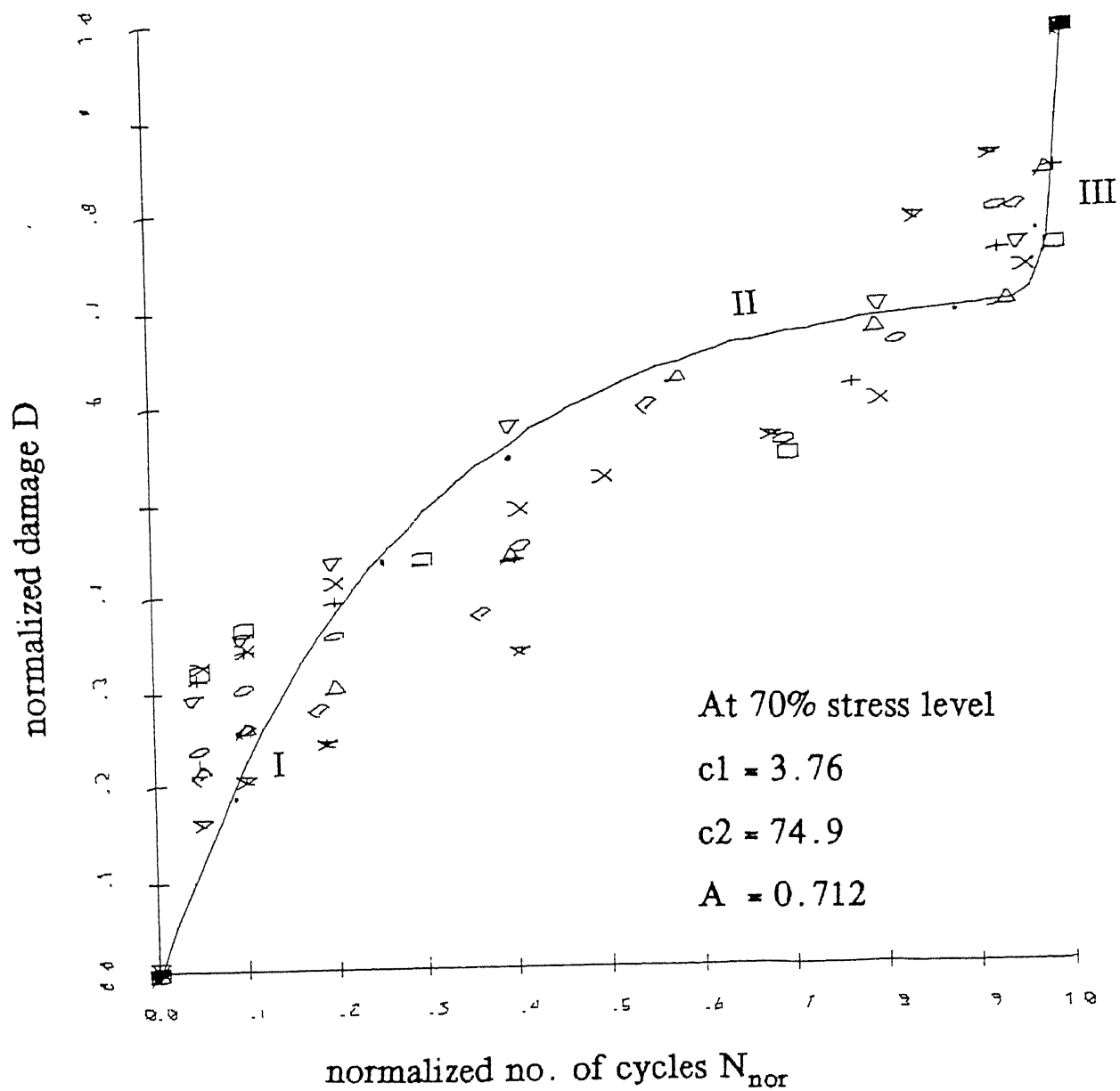


Fig. 3.10 Damage accumulation plots (each symbol represents a specimen)

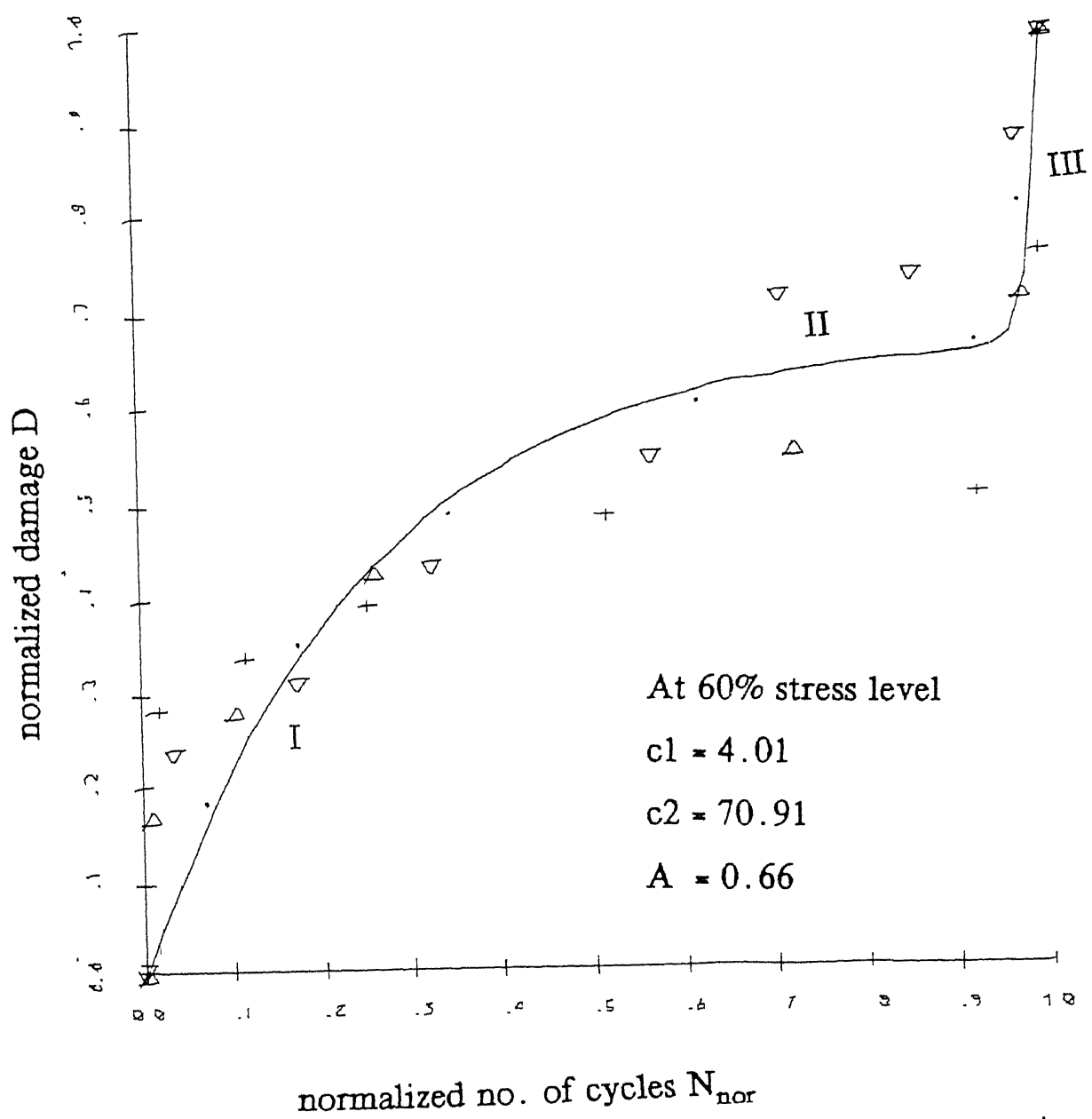


Fig. 3.11 Damage accumulation plots (each symbol represents a specimen)

cycles, and finally in stage III, the damage rate increases rapidly with the number of cycles until fracture occurs.

All the three stages, for each damage curve are clearly visible. In 90% and 80% stress levels, stage I is comparatively larger and stage II and III are comparatively smaller. In 70 & 60% stress levels stages II and III are comparatively larger and stage I is comparatively smaller. A further exploration of the figures reveals that, at lower stress levels, a larger amount of damage takes place during the last few cycles. On the other hand, at higher stress levels the amount of damage is more during the beginning for a considerable number of cycles.

3.5 S-N CURVE :

The chief purpose of most fatigue tests becomes the experimental determination of the relation between fatigue life and the magnitude of applied stress range for the material. The major attention is, therefore, accorded to these two factors, and it appears possible to condense the final result into a table, a graph or an analytical expression.

For the present investigations, normalized maximum stress (S_{max}/S_u) has been plotted against fatigue life in Fig 3.12, keeping $R = 0.1$. The nature of the curve is as expected i.e. fatigue life increases as fatigue stress decreases.

In general normalized fatigue strength can be expressed as follows,

$$S_{max}/S_u = F(N_f, R, f, T, \dots) \quad (3.8)$$

Where,

S_{max} : Maximum stress applied during fatigue cycling.

S_u : Average ultimate static strength,

N_f : Fatigue life,

R : Fatigue stress ratio,

f : Frequency of loading,

T : Temperature.

The function F has to be evaluated experimentally. It is therefore, necessary to simplify the equation to make it applicable to design analysis too. For this purpose, neglecting the effect of frequency, f , and temperature, T , and taking fatigue stress ratio R , to be a constant ($=0.1$) for present study, the equation 3.8 reduces to,

$$S_{\max}/S_u = F(N_f) \quad (3.9)$$

The nature of the function, F , has been suggested by a number of investigators [12,13,15,18,23,30,32,36] for developing analytical model for S-N curve. However, it has been observed that the S-N curve of composite materials can often be represented by a Linear law with fatigue life on log scale [12,18,36],

$$S_{\max}/S_u = m \log_{10} N_f + 1 \quad (3.10)$$

Where,

$m, 1$: Material constants.

Another useful relationship to represent fatigue data is power law [13,18],

$$(S_{\max} / S_u) N_f^a = b. \quad (3.11)$$

Where,

a, b : Other material constants.

Hwang & Han [15] developed the following useful

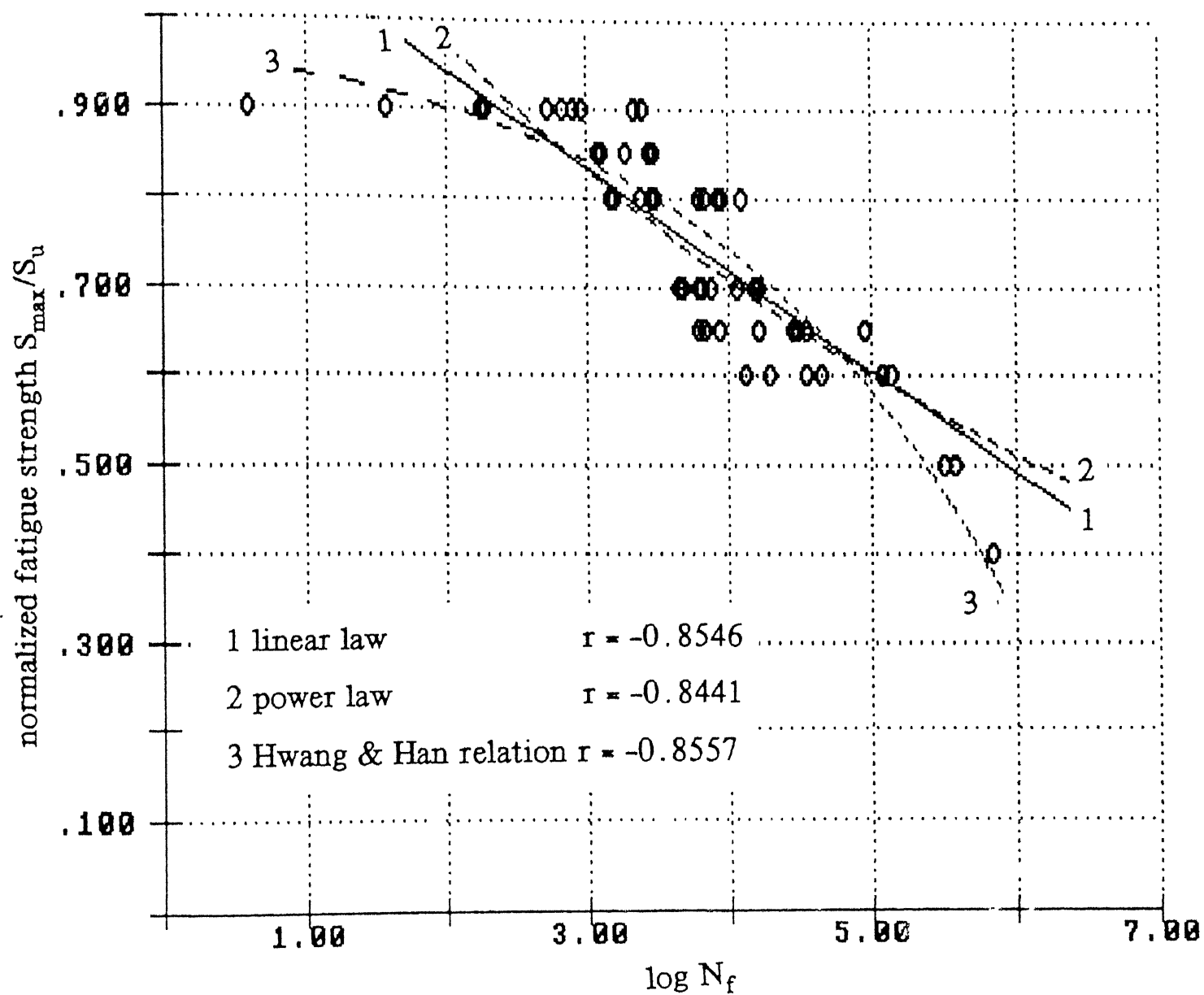


Fig. 3.12 S_{\max}/S_u - $\log N_f$ curve.

relationship to represent fatigue data using fatigue modulus concept and strain failure criterion.

$$N_f = [c (1 - S_{\max} / S_u)]^{1/d} \quad (3.12)$$

In above equations material constants are not universal. Hence they are found experimentally. For the present case, constants were found by fitting the equations to experimental data by the least square method. The coefficient of correlation r , between experimental data is also found for each case.

Linear law;

$$m = -0.1138, \quad l = 1.172, \quad r = -0.8546$$

Power law;

$$a = 0.0706, \quad b = 1.35, \quad r = -0.8441$$

Hwang & Han relation;

$$c = 26.91, \quad d = 0.210, \quad r = -0.8557$$

The coefficient of correlation r for Hwang & Han relation is slightly higher than that of Linear law. But by seeing the trend of these curves Linear law seems to be better. The fatigue strength found from Linear law, at $N = 10^6$ is about $0.489 S_u$ with no indication of an apparent endurance limit.

3.6 PROBABILITY S-N CURVE (ANALYSIS OF SCATTER OF FATIGUE DATA) :

Due to large scatter of composite material properties, especially the fatigue life, statistical methods are necessary to analyze experimental data & predict properties. Therefore it is necessary to think in terms of the probability of a specimen attaining a certain life at a given stress or the probability of failure at a given stress in the vicinity of the fatigue limit.

This requires testing of considerably large no. of samples so that the statistical parameters for estimating probabilities can be determined. The basic method for expressing fatigue data should then be adequate to represent the relationship between stress, no. of cycles to failure, and probability of failure. The reason of scatter as found by many investigators [14,28] are,

1. Batch-to-batch variation of resin, fiber and sizing.
2. Local variation of resin cure, resin content or fiber distribution, and fiber orientation within a piece.
3. Piece-to-piece variation due to resin flow, air bubbles, wrinkles, fiber joints.
4. Difference in environmental conditions as temperature (elevated temperature magnifies the scatter), moisture content, etc.

Different investigators have estimated the data scatter assuming different distributions, such as log normal [14,20] and Weibull [18,23,25,30,31,32,34] distributions. Most of the investigators found the two parameter Weibull distributions as the best distribution for the fatigue data analysis. The three parameter weibull distribution has the difficulty of having negative position parameter i.e. possibility of getting negative fatigue life which is not practical. Therefore, present scatter in the life data is analyzed by the two parameter weibull distribution,

$$P(x \leq X) = 1 - \exp \left[- \left(\frac{X}{\beta} \right)^\alpha \right] \quad (3.13)$$

Where,

P : Unreliability or probability of failure at X i.e. the

probability of a random variable, x , being less than a particular value, X ,

α : Shape parameter,

β : Scale parameter,

It is observed that there are several ways of analyzing the data with the Weibull model by selecting the random variable, x , in different ways [18,23,25,30,32,34]. One of the way, described by Hahn and Kim [18] and supported by Sims et.al. [23], selected for the present analysis is as follows,

$$X = N_{fnor} = N_f / N_{fth} \quad (3.14)$$

where,

N_{fnor} : normalized fatigue life,

N_f : fatigue life,

N_{fth} : theoretical fatigue life predicted from one of the Eq.3.10 - 3.12 for a particular stress or strain.

Thus Eq. 3.13 can be rewritten as,

$$P = 1 - \exp [- (N_{fnor} / \beta)^\alpha] \quad (3.15)$$

where,

P : probability of fatigue life being shorter than N_f at the particular stress or strain for which N_{fth} is calculated.

From normalized fatigue life, N_{fnor} , the shape and scale parameters can be estimated by simple regression analysis. This technique requires an assignment of numerical values of P_i (called the rank) for each experimental point $N_{fnor i}$. There are

many ways of making this assignment, but in this study the median rank method, as used by Chou et.al. [37], is used. Here the experimental points, $N_{fnor\ i}$, are ordered from lowest to highest and then experimental P_i is assigned by the approximate median rank formula,

$$P_i = \frac{i - 0.3}{n + 0.4}, \quad i = 1, 2, \dots, n \quad (3.16)$$

where,

n : total number of experimental points.

In using linear regression the Eq. 3.15 can be transformed by taking the logarithm twice, into the form,

$$y = \alpha x - \alpha \ln \beta \quad (3.17)$$

where,

$$x = \ln N_{fnor} \quad (3.18)$$

$$y = \ln \ln (1 / 1 - P) \quad (3.19)$$

For each experimental $N_{fnor\ i}$, the corresponding values of x_i 's are evaluated by Eq. 3.18 and for each experimental rank value, P_i , experimental y_i 's are evaluated from Eq. 3.19. The theoretical values of y_{ti} 's, associated with the theoretical distribution (Eq. 3.15), are evaluated by Eq. 3.17 at each experimental x_i 's. The difference $y_i - y_{ti}$, which represents the error, is squared and summed over i as,

$$\begin{aligned} \delta^2 &= \sum_{i=1}^n (y_i - y_{ti})^2 \\ &= \sum_{i=1}^n (y_i - \alpha x_i + \alpha \ln \beta)^2 \end{aligned} \quad (3.20)$$

This sum of the square of errors is then minimized by forming the two equations,

$$\frac{\partial \delta^2}{\partial \alpha} = 0 \quad (3.21)$$

$$\text{and} \quad \frac{\partial \delta^2}{\partial \beta} = 0 \quad (3.22)$$

Solving these two equations yields the two unknown parameters as,

$$\alpha = \frac{\sum_{i=1}^n x_i y_i - 1/n \sum_{i=1}^n x_i \sum_{i=1}^n y_i}{\sum_{i=1}^n x_i^2 - 1/n \left(\sum_{i=1}^n x_i \right)^2} \quad (3.23)$$

$$\beta = \exp \left[\frac{\alpha \sum_{i=1}^n x_i - \sum_{i=1}^n y_i}{n \alpha} \right] \quad (3.24)$$

Although, the shape parameter, α , may change with the fatigue stress or strain. Due to limited number of experimental points at each stress level, α is assumed independent of fatigue stress. The data at various stress levels can, then, be pooled to estimate single shape and scale parameters.

Scatter in fatigue life is shown in Fig. 3.13 using $\ln(N_f/N_{fth})$ and $\ln \ln (1/1-P)$ as the parameters along the x and y axis respectively. A straight line is fitted by minimizing sum of the square of errors. The experimental points $N_{f \text{ nor } i}$'s and P_i 's are plotted in Fig. 3.14 along with the theoretical curve (Eq. 3.15) associated with fatigue stress linear law (Eq. 3.10). The theoretical distribution curve fits the data quite well,

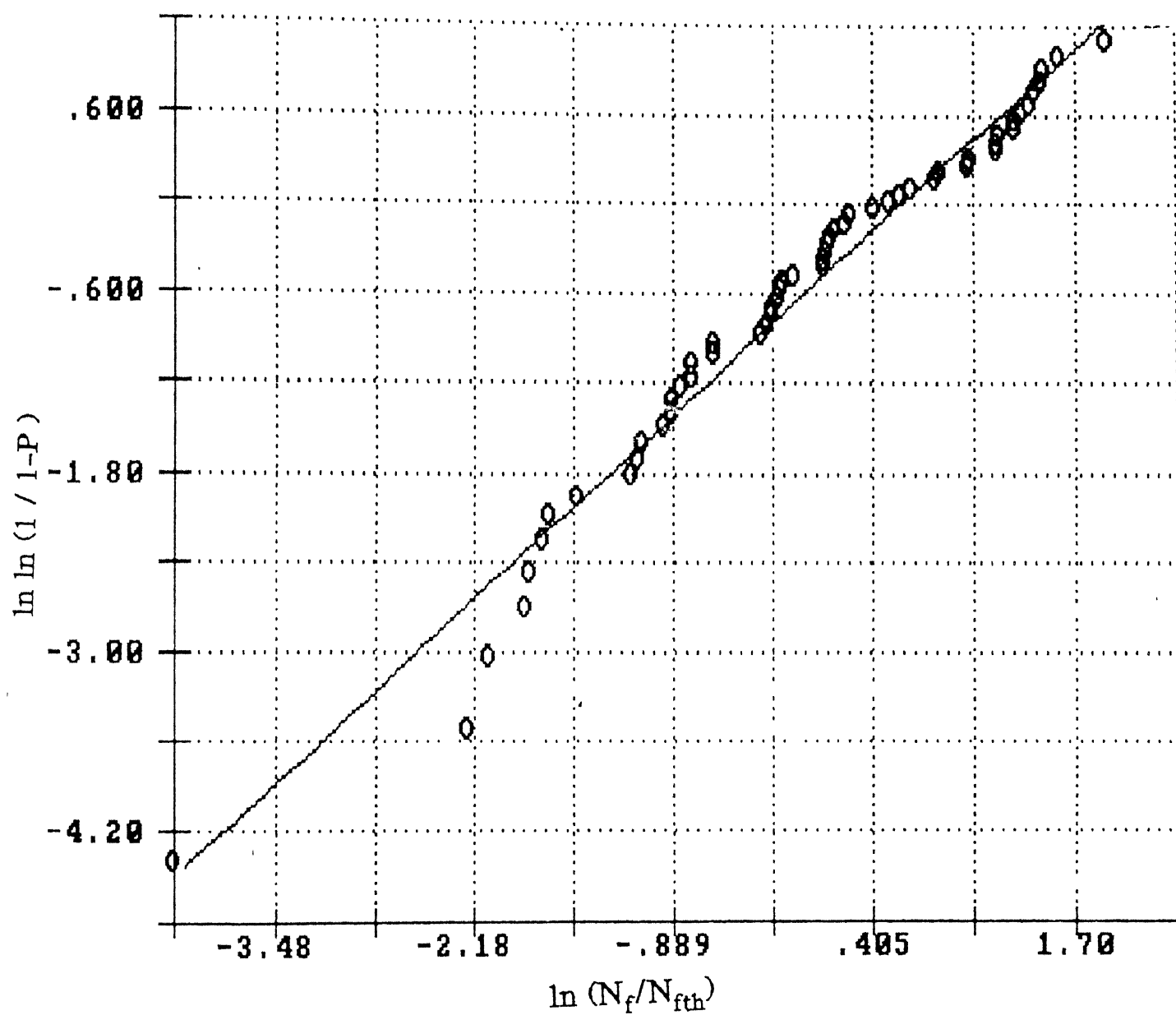


Fig. 3.13 Scatter in fatigue life.

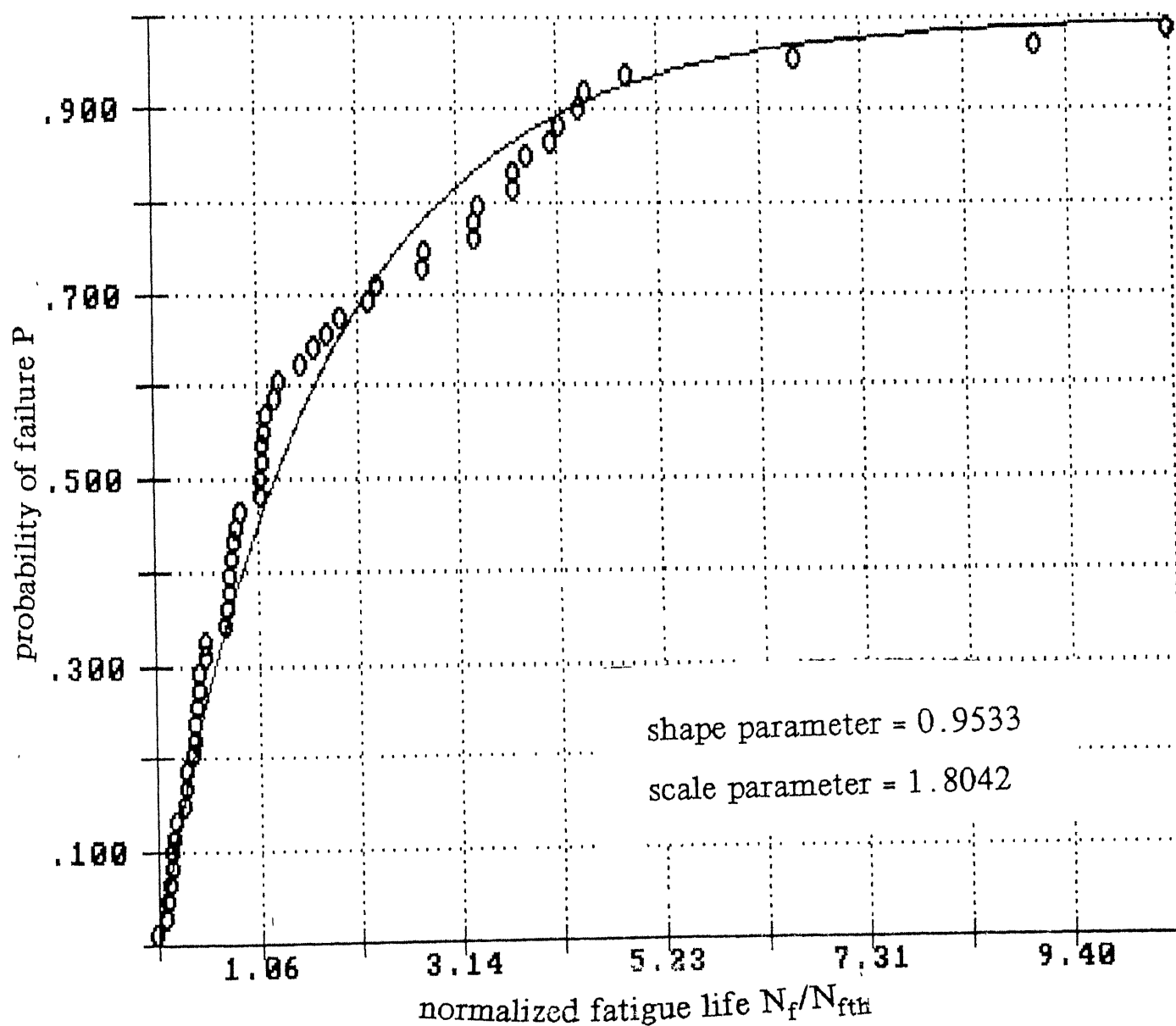


Fig. 3.14 Cumulative probability distribution curve.

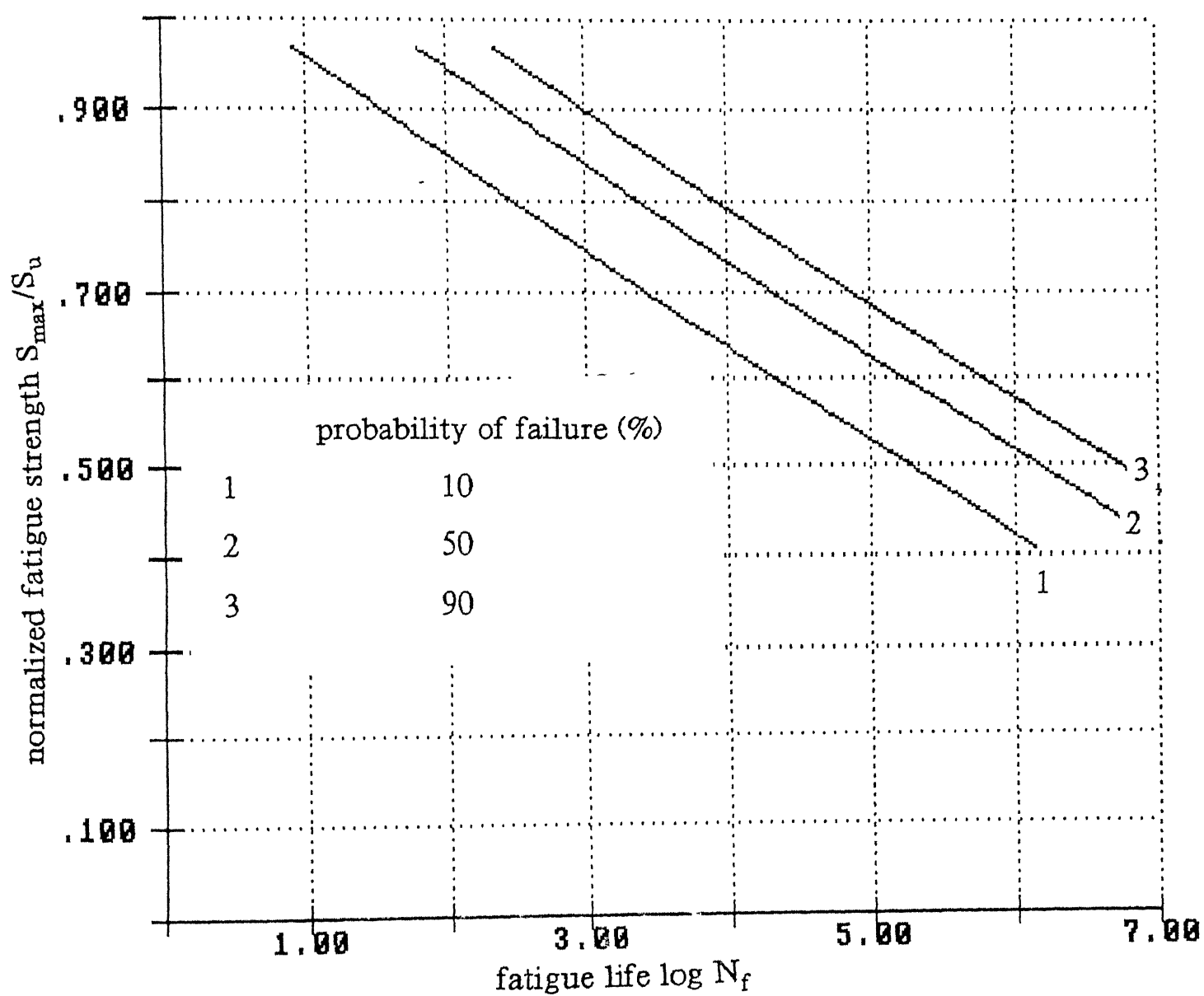


Fig. 3.15 P - S - N curve.

which assures the use of Weibull distribution. Similar curves associated with Eq. 3.11 - 3.12 can be drawn.

Commonly it is required to find out the fatigue life corresponding to some fatigue stress or strain with some probability of failure. It is, therefore, required to draw a P-S-N curve on normalized fatigue stress versus log of fatigue life coordinate, keeping probability as parameter. A P-S-N curve for fatigue stress linear law (Eq. 3.10) correlating Fig. 3.12 and Fig. 3.14 is drawn in Fig. 3.15, for the three probabilities of failure, namely 10, 50, and 90 percent.

3.7 Microscopic study of damage during fatigue :

Development of damage was studied for two specimens each at stress levels of 90% and 70% through microscopic examinations of one edge of the specimens. For this purpose one edge of the specimen was polished. The polishing was carried out by conventional metallographic technique. The final stage of polishing was carried out on a rotary polisher covered with velvet cloth and using water mixed with alumina powder as the abrasive. The microscopic examination was carried out at three locations marked along the specimen length before the test was started. The polished edge was examined, before loading and at intermediate fatigue cycles, with the help of an image analyser at a magnification of 170X. Examinations were carried out by traversing the specimen along transverse direction throughout the thickness at marked places. Microstructure of the specimen was directly seen on a 170 X 135 mm² screen of the image analyser. The screen was divided in small squares of 3 mm side, using a

transparency.

Examinations of the samples before loading revealed the presence of voids. The voids had the appearance of elongated bubbles, which are caused by air entrapped in the fabric and resin during fabrication. It was found from examination of the polished edge, that the outer fabric layer was damaged at the outward crest of the longitudinal fibre as can be observed from photograph in Fig. 3.22 b. This damage resulted during cutting of the laminates to the desired size.

Examination of fatigue specimens showed that matrix cracks occur randomly and size of matrix crack increases with increase in number of cycles. The photographs showing matrix crack, debonding, fiber breaking and other features are presented in Figs. 3.22 to 3.24. Debonds were generally first found to occur from the end of transverse fibers at crest of longitudinal fibers as shown in Figs. 3.22 d & 3.23 a. These debonds propagated along longitudinal fibers. At higher cycles, it became difficult to count matrix cracks & debonds due to dull picture of the edge as shown in Fig. 3.24 a. At this stage, some of matrix cracks coalesce with debondings. Fibers within bundles also get separated. Further, longitudinal fibers come out of the polished edge as shown in Fig. 3.24 a. These were predominant at 70% stress level whereas at 90% stress level these were much less. These creates problem in counting debonds and matrix cracks in final stages.

Photograph of specimens failed during tensile and fatigue tests are shown in Fig. 3.25. All specimens failed within the gauge length as desired. During fatigue tests, all the layers did

not fail at the same section ; in general, the layers failed at different sections with recognizable delamination as shown in Fig. 3.25. It was observed from the specimens which had failed at different stress levels that, delamination was more at low stress levels than that at high stress levels.

Loading of the specimen will cause an internal material rearrangement and alter the mechanical characteristics [38]. It was found from fatigue tests that surface texture of the sample becomes rough. The roughness increases with increase in the no. of cycles. Specimen surface before and after fatigue loading is shown in Fig. 3.24b and Figs. 3.24c & 3.24d respectively. Obviously, there is an increase in the undulation of the surface due to fatigue loading. Fig.3.24c shows surface texture of the specimen at 90% stress level at $n/N_f = 0.736$. Surface texture of the specimen at 70% stress level, at $n/N_f = 0.536$ is shown in Fig. 3.24d. It is clear from the figure that roughness is more at 70% stress level than that of 90% stress level for given normalized cycle. It is found that roughness of the surface depends on duration of loading and is independent of normalized no. of cycle. Hence, the dependence of surface roughness is more like a creep damage.

A quantitative study of matrix cracking, debonding & fiber breaking damage was done. Matrix crack counts were generally done on the basis of length of matrix crack or no. of matrix cracks or crack density. It has been observed that the size of matrix crack increases with increase in no. of cycles. Since the width of all matrix cracks is not same, matrix crack counts were

made on the basis of total no. of rectangles enclosed by a matrix crack in the screen. Debond counts were made by the total length of debond.

Number of matrix cracks is plotted against normalized no. of cycles for 90% and 70% stress levels in Figs. 3.16 and 3.17 respectively. Matrix crack accumulates more rapidly in early stages of the test than in the later stages of the test. At 70% stress level matrix crack and debond counts could not be made at higher cycles due to the dull picture (Fig. 3.24a).

Number of debond counts is plotted against normalized no. of cycles in Figs. 3.18 and 3.19 for 90% and 70% stress levels respectively. Debonding damage increases slowly till 45% of life and subsequently it increases rapidly.

Fiber breaking damage is measured by counting number of broken fiber bundles. During fatigue cycling all the fibers in a bundle do not break simultaneously. The fibers break sequentially as the fatigue cycling progresses. Fiber breaking damage is plotted against normalized no. of cycles for 90% and 70% stress levels in Figs. 3.20 and 3.21 respectively. It is clear from the figures that small number of fiber breaking appeared at some sites till 40% of life. Subsequently number of fiber breaking damage increased rapidly at most sites.

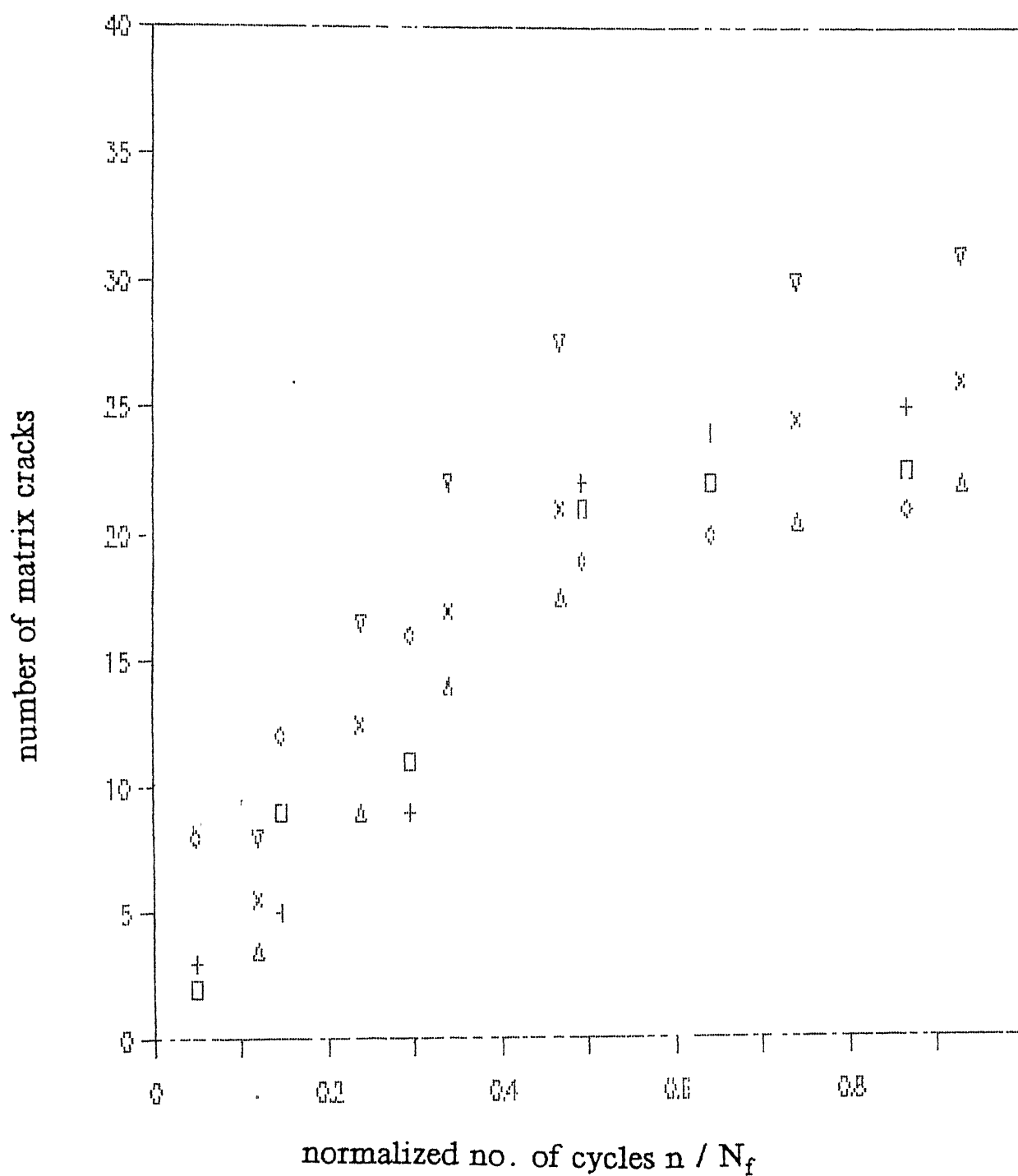


Fig. 3.16 Matrix cracking under fatigue loading at 90% stress level
(each symbol represents a representative site)

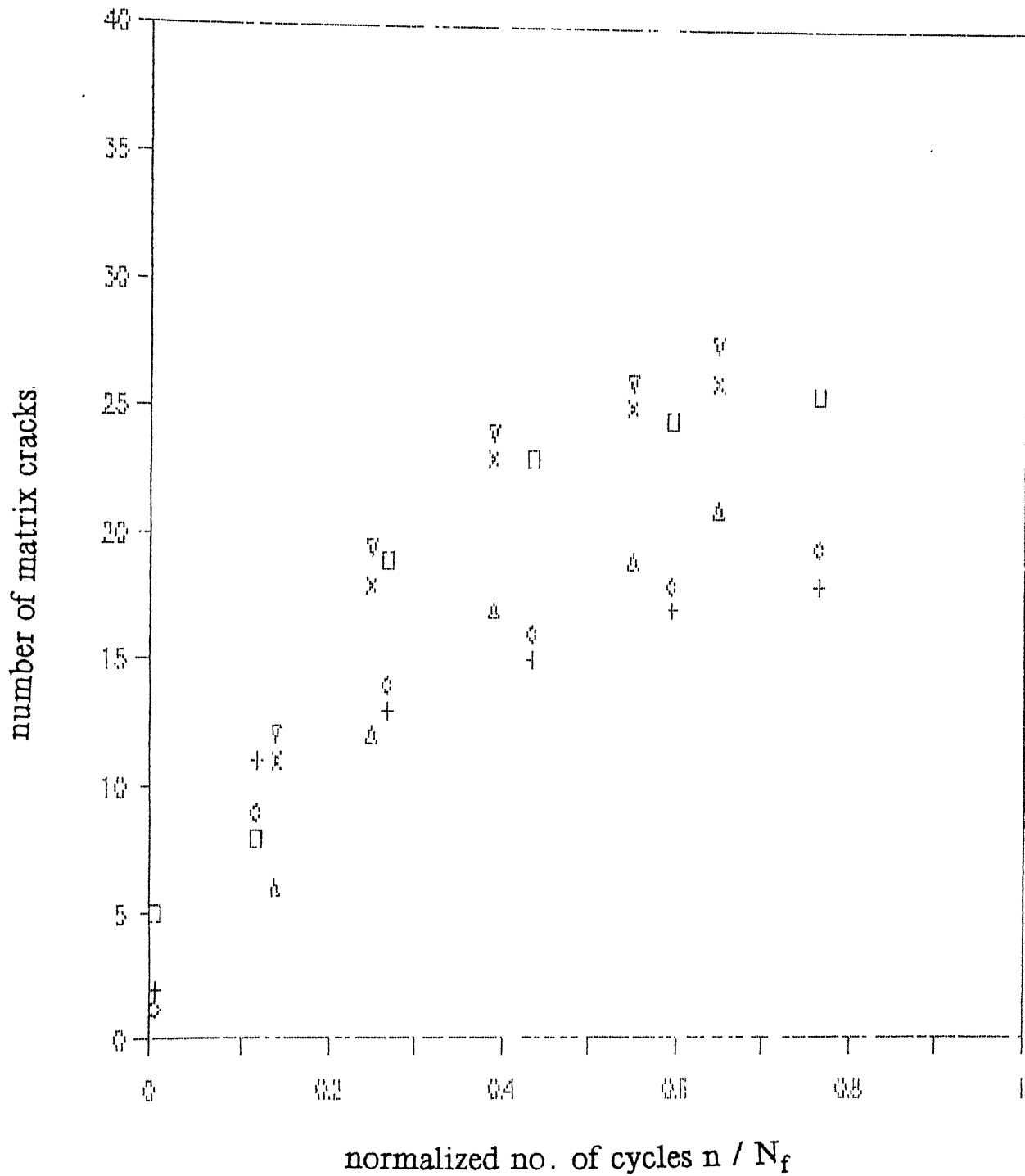


Fig. 3.17 Matrix cracking under fatigue loading at 70% stress level
(each symbol represents a representative site)

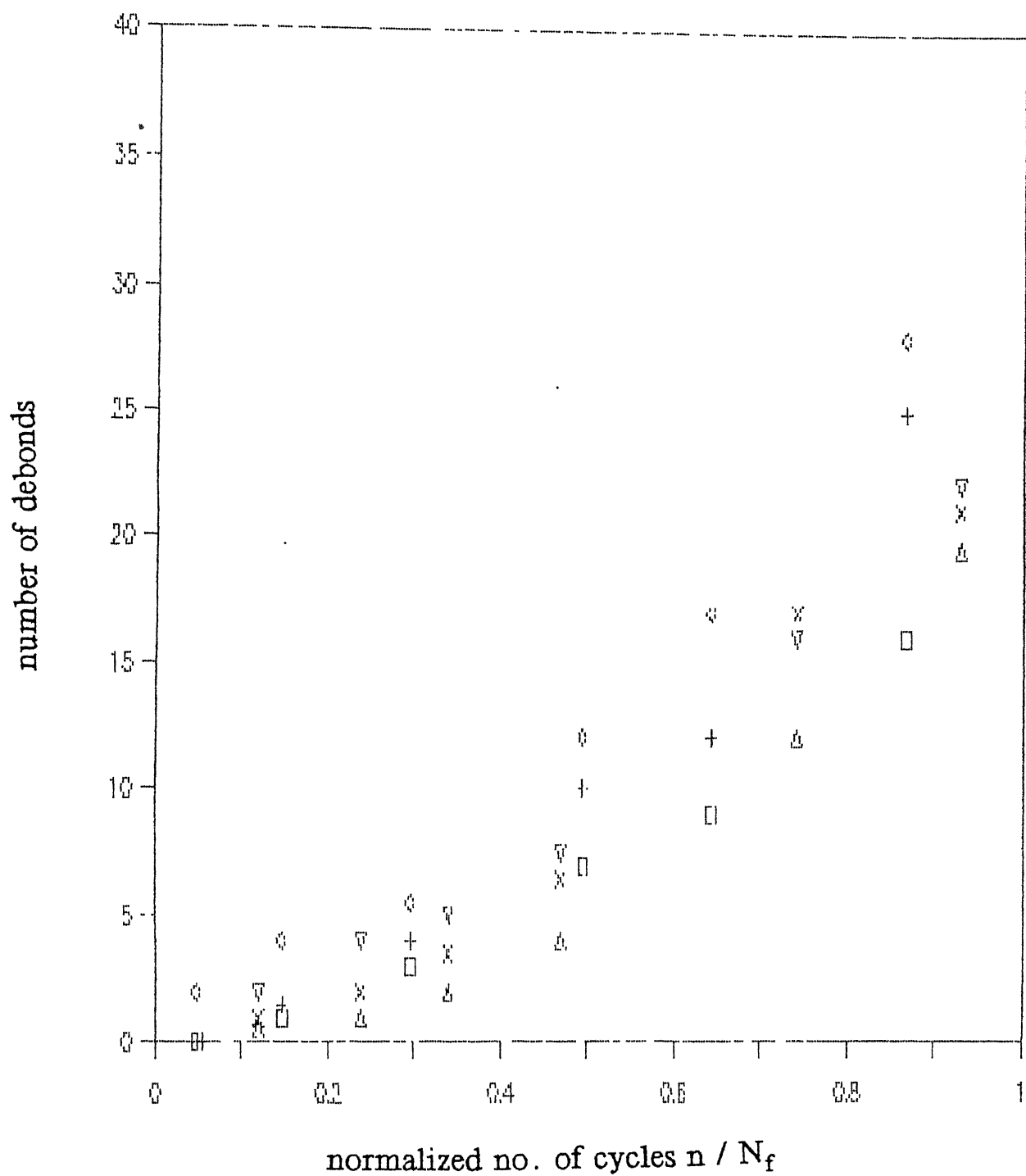


Fig. 3.18 Debonding under fatigue loading at 90% stress level (each symbol represents a representative site)

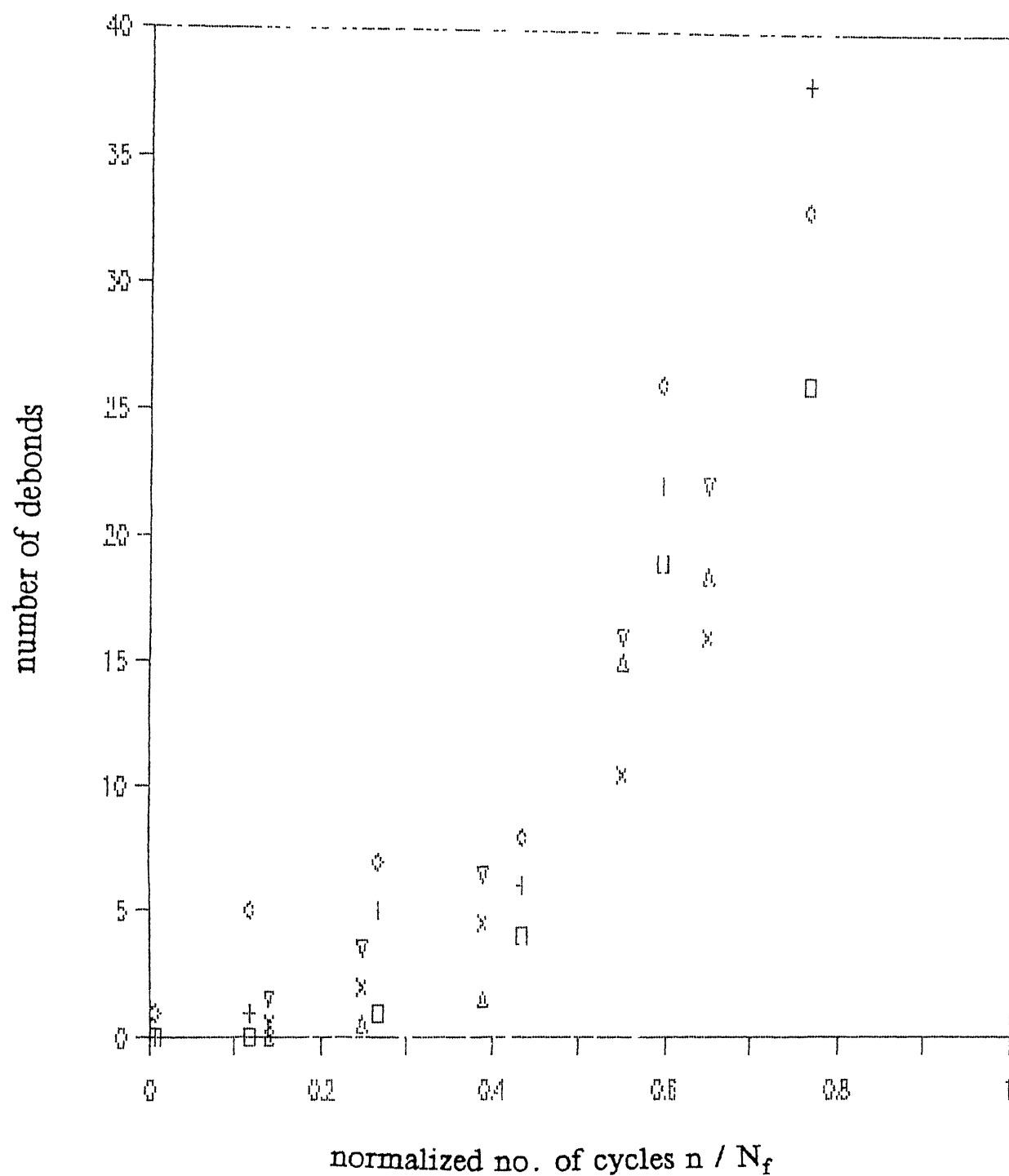


Fig. 3.19 Debonding under fatigue loading at 70% stress level (each symbol represents a representative site)

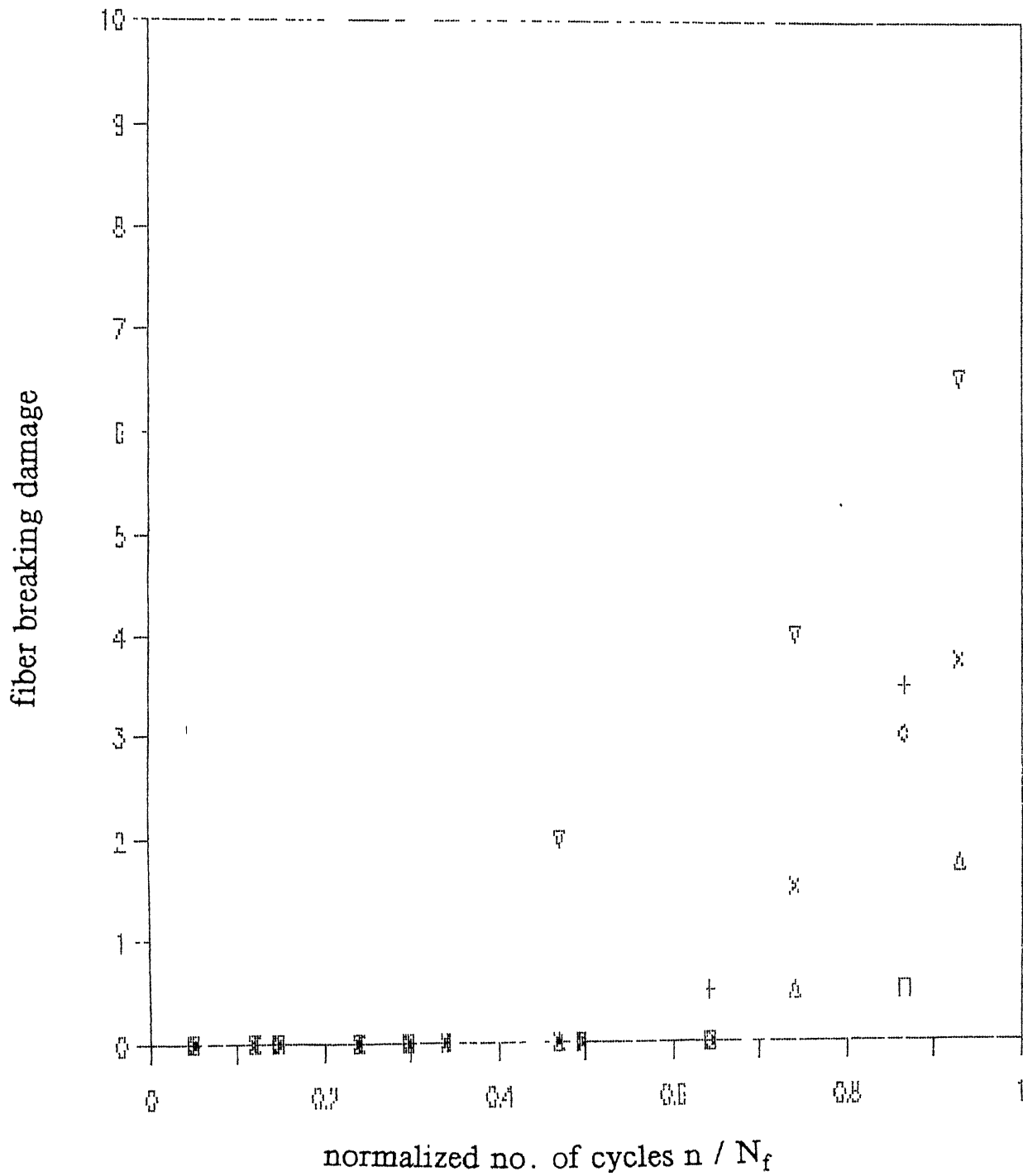


Fig. 3.20 Fiber breaking under fatigue loading at 90% stress level
(each symbol represents a representative site)

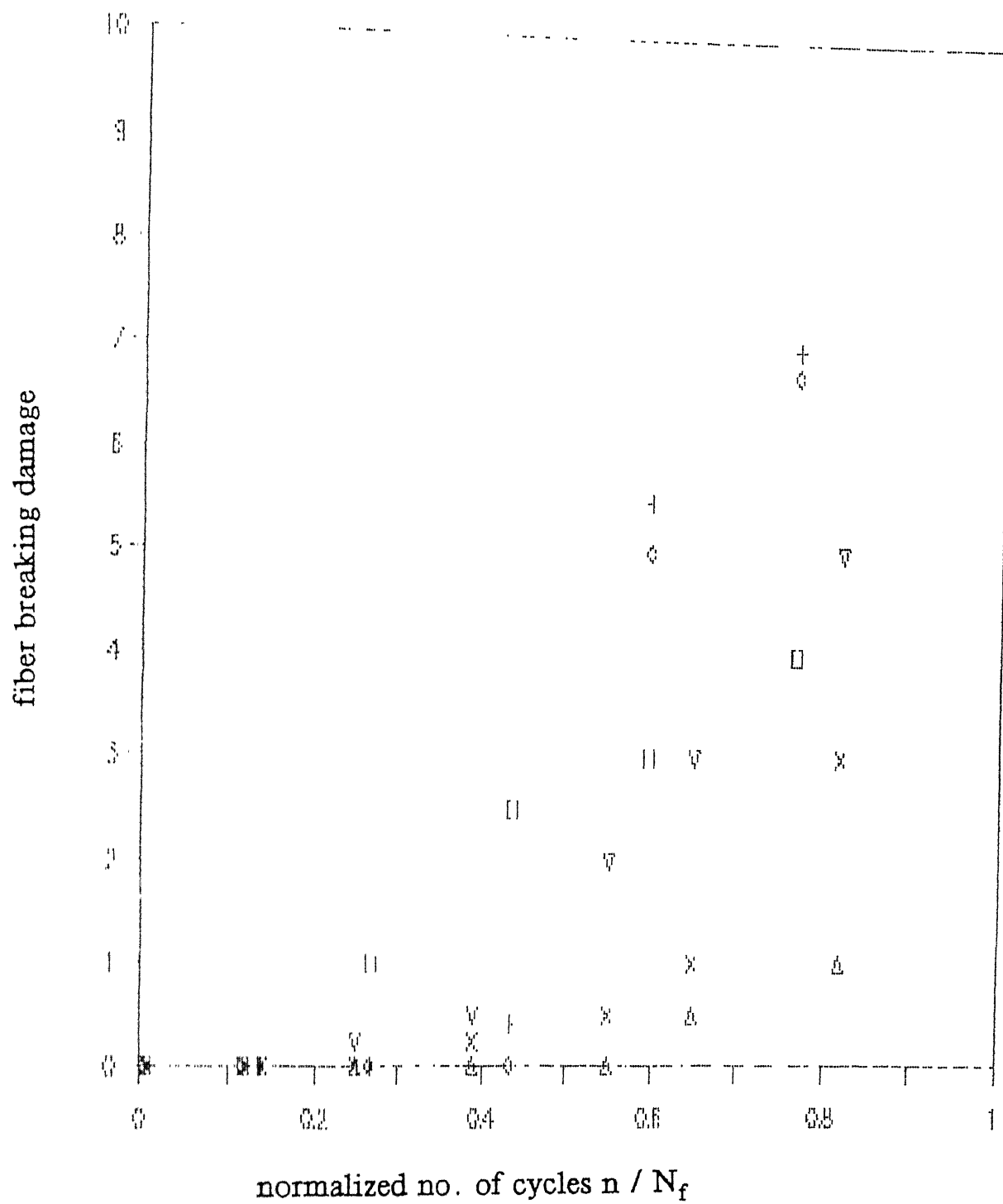


Fig. 3.21 Fiber breaking under fatigue loading at 70% stress level
(each symbol represents a representative site)

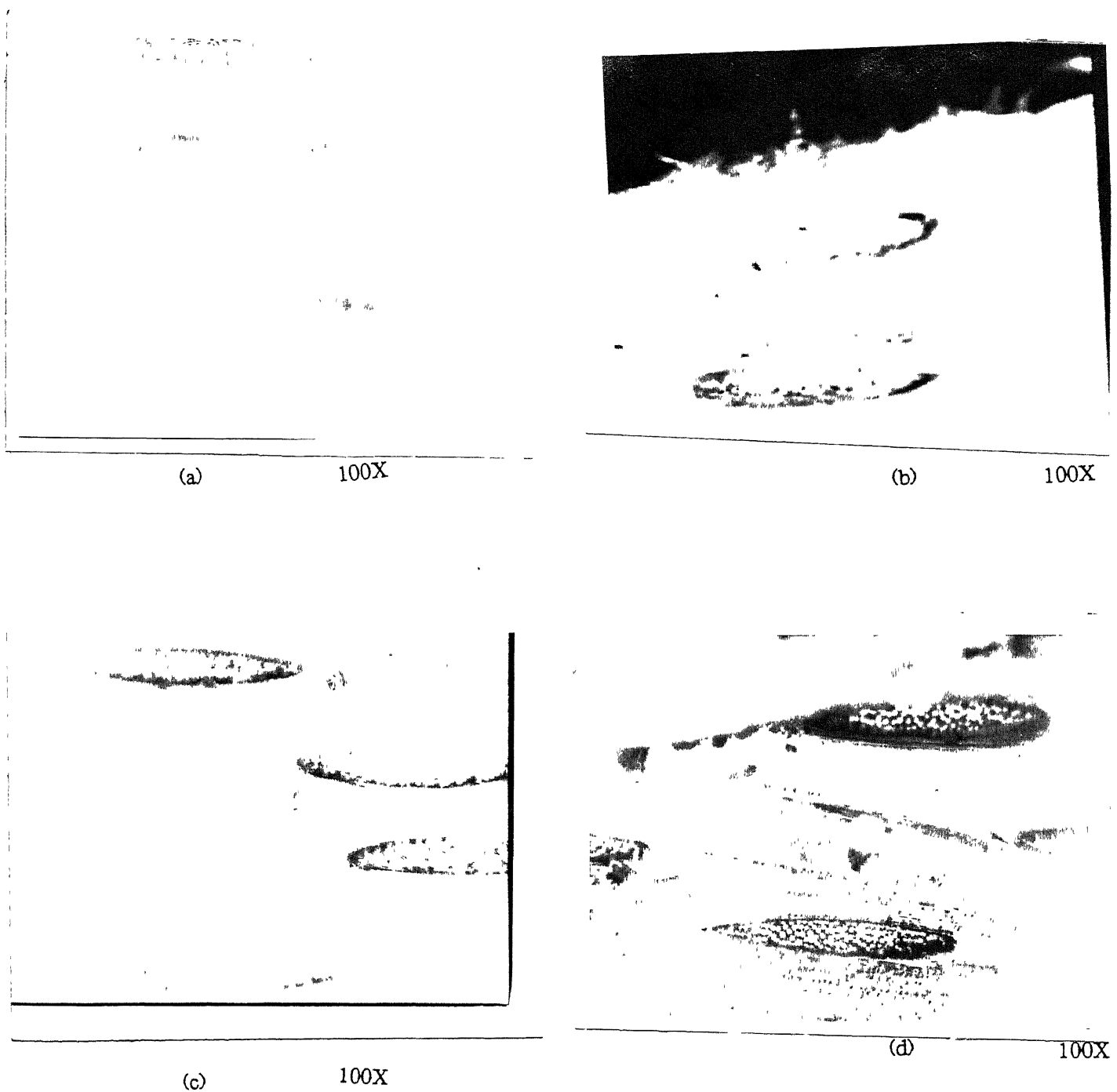
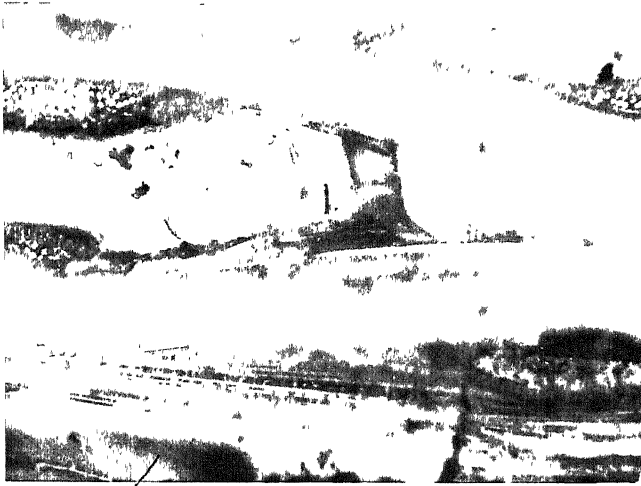


Fig. 3.22 Optical micrographs of polished edge surfaces showing

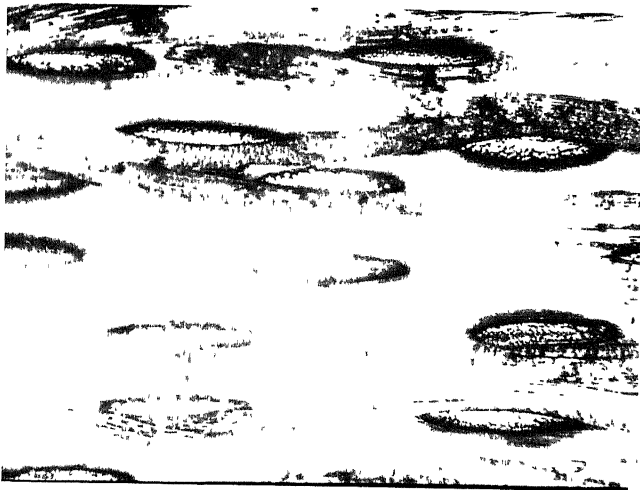
- (a) Pristine specimen.
- (b) Damaged outward fabric layer, caused during cutting of the specimen. ($n/N_f = 0.12$, 90% stress level, $N_f = 835$ cycles)
- (c) Matrix cracking damage. ($n/N_f = 0.12$, 90% stress level, $N_f = 835$ cycles)
- (d) Debonding damage. ($n/N_f = 0.536$, 70% stress level $N_f = 10350$ cycles)



(a) 100X



(b) 100X



(c) 50X



(d) 50X

Fig 3.23 Optical micrographs of polished edge surfaces showing

(a) Debonding damage & fiber separation within bundle.

($n/N_f = 0.847$, 70% stress level, $N_f = 10350$ cycles)

(b) Fiber breaking damage. ($n/N_f = 0.847$, 70% stress level, $N_f = 10350$ cycles)

(c) Surface after 1407 cycles. ($n/N_f = 0.136$, 70% stress level)

(d) Debonding damage ($n/N_f = 0.847$, 70% stress level, $N_f = 10350$ cycles)

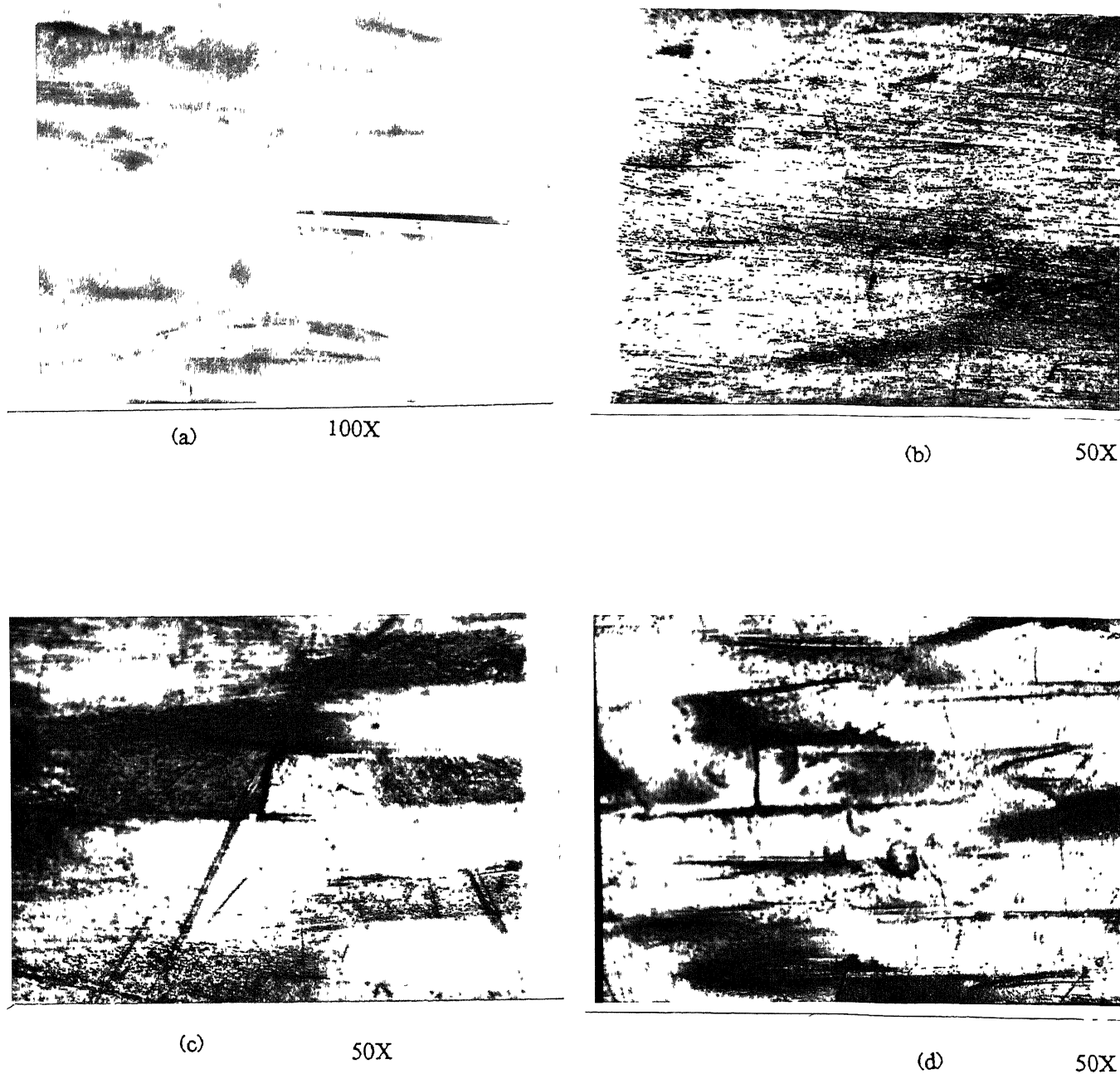
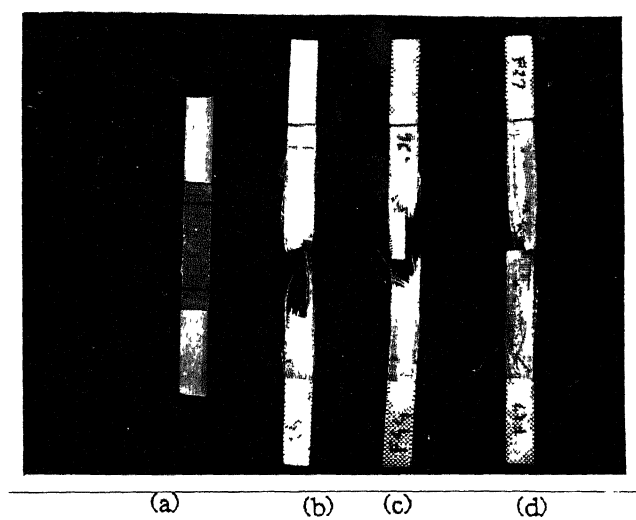
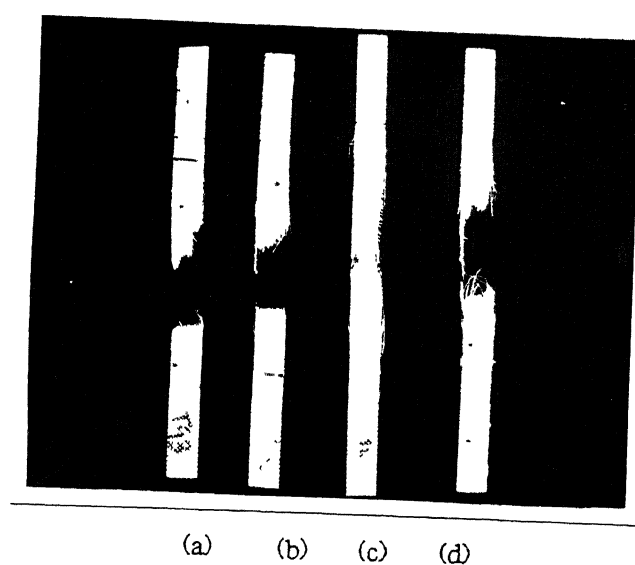


Fig. 3.24 Optical micrographs showing

- (a) Separation of fibers within bundles. Plane of longitudinal fibers has come out from the edge.
($n/N_f = 0.847$, 70% stress level & $N_f = 10350$ cycles)
- (b) Surface texture before loading.
- (c) Surface texture at 90% stress level ($n/N_f = 0.736$, $N_f = 835$ cycles)
- (d) Surface texture at 70% stress level ($n/N_f = 0.536$, $N_f = 10350$ cycles)



(1)



(2)

Fig. 3.25 (1) (a) Test specimen for tensile and fatigue tests.

(b), (c) & (d) Failed specimens during fatigue test.

(2) (a) & (b) Failed specimens during tensile test

(c) & (d) Failed specimens during fatigue test

CHAPTER 4

CONCLUSIONS AND SCOPE FOR FUTURE WORK

4.1 CONCLUSIONS :

From the results obtained during the present work, the following conclusions can be drawn:

1. During fatigue cycling of dogbone specimens, cracks are generated tangential to the neck.
2. The thickness was found to vary from specimen to specimen. This affects static strength. However, its influence on load carrying capacity per unit width and fatigue life is insignificant.
3. The stress-strain curve during tensile test is linear upto failure.
4. The variation in Young's modulus during fatigue loading for the present material is governed by re-alignment of both the fibers within the bundle as well as the molecular chains within the individual fibers.
5. The modulus of the present material increases with increase in no. of cycles. This increase in modulus reverts back to its initial value, if specimen is allowed to relax freely for 48 hrs.
6. The accumulation of damage of Kevlar fabric reinforced epoxy composite in axial fatigue can be divided into 3 stages, namely the damage initiation stage, steady damage state and the damage propagation stage. Although the damage accumulation depends on fatigue stress, it follows a definite

trend.

7. The damage accumulation can be predicted approximately by a damage model, consisting of two terms, a monotonically decreasing damage rate term and the other increasing damage rate as follows,

$$D = A \left(1 - \frac{e^{c_1(1-N_{nor})} - 1}{e^{c_1} - 1} \right) + (1 - A) \left(\frac{e^{c_2 N_{nor}} - 1}{e^{c_2} - 1} \right)$$

Where,

c_1, c_2 : constants,

A : Weighing constant.

D : Normalized damage,

$$D = \frac{F(1) - F(N)}{F(1) - F(N_f)}$$

$F(N)$: The fatigue modulus at N^{th} number of cycles,

N_f : Number of cycles to failure, i.e. fatigue life.

N_{nor} : Normalized number of cycle,

$$N_{nor} = \frac{N - 1}{N_f - 1}$$

8. The $S - N$ curve has been represented by Linear Law, Power Law, and Hwang-Han relation between normalized fatigue stress and logarithm of fatigue life. For the present case Linear Law is found to be best.
9. The scatter in fatigue life has been analysed by two parameter Weibull distribution.
10. Microscopic study of the specimen can be done effectively with the help of an Image Analyser.
11. Matrix crack damage accumulates more rapidly during early

stages of the fatigue test than in the later stages. Debonding and fiber breaking damage increases slowly during early stages of the test and increases rapidly in the final stages.

12. Surface texture of the specimen becomes rough with fatigue cycling. The amount of roughness depends on duration of fatigue loading.

4.2 SCOPE FOR FUTURE WORK :

1. Fatigue of specimens should be done at low stress levels to find the endurance limit.
2. The effect of stress level on fatigue life data scatter distribution could be found out by testing more specimens at each stress levels.
3. Damage model can be obtained for GFRP and CFRP taking fatigue modulus as damage parameter.
4. Microscopic study of some specimens at low stress levels should be done to find out the trend for matrix cracking, debonding and fiber breaking damage at different stress levels.
5. Delamination study of specimens during fatigue loading should be done.

REFERENCES

- [1] L.Penn, H.A.Newey and T.T.Chiao, " Chemical characterization of a high performance organic fiber," J. Mat. Sci. 11, 190 (1976).
- [2] C.C.Chiao and T.T.Chiao, " Aramid fibres and composites." Handbook of composites edited by George Lubin.
- [3] M.J.Salkind, " Fatigue of composites, " Composite materials: Testing and Design (Second conference)," ASTM-STP 497, P.143-169, 1972.
- [4] K.H.Boller, " Fatigue characteristics of RP laminates subjected to axial loading," Mod. plast, V41, P.145, 1964.
- [5] B.D.Agarwal & L.J.Broutman, Analysis & Performance of fiber composites, A wiley Interscience Publication, 1980.
- [6] L.H.Miner, R.A.Wolffe & C.Z.Zweben, "Fatigue, creep & impact resistance of aramid fiber reinforced composites, composite reliability," ASTM STP 580, P.549-59, 1975.
- [7] M.A.Hamstad & T.T.Chiao, "Acoustic emission from stress rupture & fatigue of an organic fiber composite," ASTM-STP 580, P.201, 1975.
- [8] A.R.Bunsell,"The tensile & fatigue behaviour of Kevlar-49 (PRD-49) fiber" J.Mat.Sci. V10, P.1300, 1975.
- [9] H.L.Ganczakowski, P.A.Smith & P.W.R.Beaumont, "On the modulus of KFRP Laminates in static & Fatigue loading," ICCM & ECCM edited by F.L. Matthews et.al. Vol.3. Page 3.166 (1987).
- [10] Linda L. Clemants, "Problems in testing ,aramid/epoxy composites" Failure modes in composites IV, edited by J.A.Cornie & F.W.crossman, P.176-183, A publication of the Metallurgical society of AMIE, 1979.

- [11] Clements, L.L., and Chiao, T.T., "Engineering design data for an organic-fiber/Epoxy composite," Composites (1977), V8, P.87.
- [12] J.W.Dally and B.d.Agarwal, "Low cycle fatigue behavior of glass fibre reinforced plastics," Proceedings of the Army symposium on solid Mechanics, AMMRC-MS 70-5, 1970.
- [13] C.K.H.Dharan, "fatigue failure mechanisms in a unidirectionally reinforced composite material," Fatigue of composite materials, ASTM-STP 569, P.171-188, 1975.
- [14] H.C.Kim and L.J.Ebert, "Fatigue life limiting parameters in fibre glass composites," J. Mat. Sci. V14, P.2616, 1979.
- [15] W.Hwang and K.S.Han, "Fatigue of composites-Fatigue Modulus concept & Life prediction," J.Comp.Mat. V20, P.154, March 1986.
- [16] T.Tanimoto and S.Amijima, "Progressive nature of fatigue damage of glass fiber reinforced plastics," J. comp. Mat. V9, P.380, Oct. 1975.
- [17] T.Tanimoto and S.Amijima, "Fatigue properties of liminated glass fibre composite materials," SPI, 29th Annual technical conference, Washington, D.C.Section 17-B, Feb. 1974.
- [18] H.T.Hahn and R.Y.Kim " Fatigue behaviour of composite laminate," J. Comp. Mat. Vol. 10, P.156, April 1976.
- [19] W.Hwang and K.S.Han " Cumulative damage models and multi-stress fatigue life prediction " J. Comp. Mat. Vol. 20, P.125, March 1986.
- [20] M.J.Owen, T.R.Smith and R.Dukes, " Failure of glass reinforced plastics, with special reference to fatigue, " plastic and polymers, P. 227, June 1969.

- [21] B.D.Agarwal and S.K.Joneja, " Flexural fatigue of a unidirectional composites in the longitudinal direction, " Mat. Sci. and Engg. V46, P.63, 1980.
- [22] C.K.H.Dharam, " Fatigue failure mechanism in pultruded graphite polyester composites, " Scientific research staff, Ford motor company, Tech. Report No. SR-74-71, June 1974.
- [23] D.E.Sims and V.H.Brogdon, " Fatigue behaviour of composites under different loading modes," Fatigue of filamentary composite materials, ASTM-STP 636, P. 185-205, 1977.
- [24] T.K.O'Brien and K.L.Reifsnider, " Fatigue damage evaluation through stiffness measurements in Boron-epoxy laminates, " J. Comp. Mat. V15, P. 55, Jan. 1981.
- [25] P.C.Chou and Robert Croman, " Degradation and Sudden-death models of Fatigue of graphite/epoxy composites, " ASTM STP 674, P. 431-454. 1979.
- [26] M.J.Owen and R.J.Home " The accumulation of damage in a glass reinforced plastic under tensile and fatigue loading " J. Phys. D. Appl. Phys. Vol 5, 1972.
- [27] H.C.Kim and L.J.Ebert. " Axial Fatigue sequence and mechanisms in unidirectional fibre glass composites," J. Comp. Mat. Vol. 20 P. 139 April 1978.
- [28] T.K.James, F.J.Appl and C.W.Bert. "Low cycle Fatigue of a glass-fabric-reinforced plastic laminate," Experimental Mechanics, V8, P.327.
- [29] W.Hwang and K.S.Han, "Statistical study of strength & fatigue life of composite materials," composites. Vol.18. P.47, No 1, Jan.1987.
- [30] G.P.Sendeckyj, "Fitting models to composite materials

- fatigue data," ASTM STP 734. P.245-260, 1981.
- [31] P.C.Chou and R.Croman, "Scale effect in fatigue of composite materials," J. Comp. Mat. V13, P.178, July 1979.
- [32] H.T.Hahn, "Fatigue behaviour & life prediction of composite laminates," Composite materials: Testing & Design (Fifth conference), ASTM-STP 674, P.383-417, 1978.
- [33] M.M.Schwartz, composite material hand book, Mc Graw-Hill book company, 1984.
- [34] J.N.Yang and D.L.Jones, "Statistical fatigue of Graphite/Epoxy angle ply laminates in shear," J. Comp. Mat. V.12, P.371, Oct. 1978.
- [35] B.D.Agarwal and Bharat Bhushan, "Flexural fatigue behaviour of Kevlar fabric reinforced epoxy resin composites," M.Tech.Thesis. Dept. of Mech. Engg. I.I.T. Kanpur.
- [36] B.D.Agarwal and J.W.Dally, "Prediction of Low-cycle Fatigue behaviour of GFRP: an experimental approach," J. Mat. Sci. Vol 10, No.1, P. 193-99, 1975.
- [37] C. Zweben, "The Flexural strength of aramid fiber composites," J. Comp. Mat. Vol.12, P. 422, October 1978.
- [38] Ryszard Pyrz "Strength reduction of woven glass fabric composite after creep deformation," ICCM and ECCM edited by F.L.Mathews et.al. Vol. 4, Page 4.272 ,1987.
- [39] Morgan, R.J., Mones, E.T., Steele, W.J., Deutschman, S.B., "The failure modes and durability of Kevlar/epoxy composites," In Proc. 12th National SAMPE conference, Seattle, Washington, 1980.
- [40] J.T.Fong "What is fatigue damage," Damage in composite materials, ASTM STP 775, P.243 , 1982.